International Journal of Biological Macromolecules 335 (2026) 149205

Contents lists available at ScienceDirect

International Journal of Biological Macromolecules

journal homepage: www.elsevier.com/locate/ijbiomac

Biomimetic core-shell breast cancer models using alginate, gelatin, and collagen I: simulating the tumor matrix for drug evaluation

Uxia Gato-Diaz [a], Lisandra de Castro-Alves [b,c], Angel Concheiro [a,c], Yolanda Piñeiro [b,c], Carmen Alvarez-Lorenzo [a,c], Barbara Blanco-Fernandez [a,c,*], José Rivas [b,c,**]

[a] I+D Farma Group (GI-1645), Department of Pharmacology, Pharmacy and Pharmaceutical Technology, Faculty of Pharmacy and Institute of Materials (iMATUS), University of Santiago de Compostela, Santiago de Compostela, 15782, Spain
[b] NANOMAG Group, Applied Physics Department, Faculty of Physics, Institute of Materials (iMATUS), University of Santiago de Compostela, Santiago de Compostela, 15782, Spain
[c] Health Research Institute of Santiago de Compostela (IDIS), Complexo Hospitalario Universitario de Santiago de Compostela, Santiago de Compostela, 15706, Spain

ARTICLE INFO

Keywords:
3D *in vitro* cancer model
Core-shell hydrogel
Drug screening
Invadopodia
Doxorubicin resistance

ABSTRACT

Breast cancer remains among the most prevalent cancers in women worldwide. During tumor development, the extracellular matrix is altered to support tumor progression and therapy resistance. Therefore, there is a need to develop breast cancer models that replicate the complex tumor extracellular matrix to accurately mimic the mechanisms by which it influences drug resistance and cancer cell malignancy. In this study, we fabricated an innovative breast cancer 3D *in vitro* model consisting of core-shell hydrogel beads from alginate, gelatin, and collagen I by extrusion through a coaxial needle. Breast cancer cells proliferated in the core of all prototypes designed, forming spheroids and cell aggregates with a high resistance to doxorubicin. The addition of Collagen I to the developed model enabled the upregulation of malignancy markers (Col1A1, Ki67, FOXC2, SNAI1, NFKB1, WWTR1), invasion markers (WASL, ACTA1, MYO1E, TPM4, PODXL, ITGA2, ITGA5, MENA, EGFR, CDC42), and drug resistance markers (ABCG2, CYP1A1, BAX, HSP90AA1) occurring *in vivo*. The developed 3D *in vitro* model can clarify the contribution of the extracellular matrix to the tumor outcome and drug efficacy by replicating some key characteristics of breast tumors, establishing a novel tool for chemotherapeutic agents and drug screening.

1. Introduction

Breast cancer (BC) is the most prevalent cancer worldwide, ranking fourth in terms of mortality and causing 670,000 deaths globally in 2022 [1]. BC includes a variety of diseases involving the growth of carcinogenic cells in different parts of the breast's glandular tissue [2]. The first stage in breast cancer is the ductal carcinoma *in situ* (DCIS), in which tumor cells proliferate uncontrollably while remaining confined within the breast ducts. DCIS can progress to an invasive stage, characterized by tumor cell infiltration beyond the ductal basement membrane and proliferation within the surrounding tissue [3]. Pharmaceutical and biotechnological industries invest significant amounts of resources in the pursuit of more effective oncology treatments. Despite all efforts, drug approval rates are still very low, mainly due to the lack of efficiency or high toxicity of the drug candidates [4]. This is mainly caused by the absence of clinically translatable preclinical models that mimic the characteristics of human breast tumors.

Nowadays, 2D *in vitro* and animal models are still the most commonly used in drug discovery. In the early stages of cancer research, 2D models are the preferred option due to their reproducibility and affordability, but they cannot replicate the cancer cell genotype/phenotype, metabolism, or interactions with other cells and the extracellular matrix (ECM) that occur *in vivo* [5]. Animal models, primarily rodent models, are also often used in preclinical studies owing to their closer resemblance to human physiology. However, the need to choose immunodeficient animals to study human diseases, as well as the

* Correspondence to: B. Blanco-Fernandez, I+D Farma Group (GI-1645), Department of Pharmacology, Pharmacy and Pharmaceutical Technology, Faculty of Pharmacy and Institute of Materials (iMATUS), University of Santiago de Compostela, Santiago de Compostela, 15782, Spain.
** Correspondence to: J. Rivas, NANOMAG Group, Applied Physics Department, Faculty of Physics, Institute of Materials (iMATUS), University of Santiago de Compostela, Santiago de Compostela 15782, Spain.
E-mail addresses: barbara.blanco.fernandez@usc.es (B. Blanco-Fernandez), jose.rivas@usc.es (J. Rivas).

https://doi.org/10.1016/j.ijbiomac.2025.149205
Received 16 May 2025; Received in revised form 5 November 2025; Accepted 21 November 2025
Available online 22 November 2025

differences between species, limit the similarities with human tumors [5]. Moreover, governmental institutions and regulatory agencies are working towards applying the principles of replacement, reduction, and refinement in animal experimentation. Overall, available models still have a long way to go to recreate the behavior of human tumors and the drug response, becoming an important limitation in the search for effective anticancer therapeutics.

Cancer 3D *in vitro* models could overcome some of the limitations of current models, enabling a closer understanding of BC and easing the investigations of new therapies [6]. Indeed, several studies have already demonstrated the potential of 3D cancer models in drug screening. These models not only better reproduce the *in vivo* response of tumors to conventional chemotherapeutics [7,8], but also to other therapeutic agents such as nanocarrier systems and targeted biologics [9,10]. The drug resistance observed in these studies underscores the importance of 3D models as clinically relevant and translational systems for drug screening, in contrast to conventional 2D cultures.

In recent years, studies involving 3D breast cancer models have focused on recapitulating the tumor microenvironment (TME), which plays an important role in tumor progression and drug efficacy. The breast TME is formed by a mass of heterogeneous breast cancer cells (BCCs) with abnormal growth, the ECM, infiltrating stromal cells, and soluble factors [5,11]. During tumor progression, the ECM is constantly changing to promote tumor growth and metastasis. Some of these changes are the increase in fibrillar proteins, such as collagen type I (Col1), and changes in its stiffness, porosity, and permeability [12]. All these changes also promote drug resistance. Diverse pathways, such as drug resistance and antiapoptotic pathways, can be activated due to hypoxia, metabolic stress, and ECM physical properties [13].

The importance of the ECM has motivated the creation of 3D *in vitro* models that replicate the ECM through a scaffold-based approach. Hydrogels are the most suitable scaffolds due to their biocompatibility and similarities with the ECM's viscoelastic properties. Moreover, they can be designed to create artificial tumors [5,13]. Hydrogel physicochemical properties can be modulated using different polysaccharides (alginate, hyaluronic acid, *etc.*), proteins (Col1, gelatin methacrylate, *etc.*), synthetic polymers (polyethylene glycol), and native ECMs (Matrigel) [5]. Col1 is a highly expressed protein in the breast TME, which enhances ECM stiffness and desmoplasia development [14]. For this reason, Col1 hydrogels have been employed for investigating tumorigenesis, drug screening [15,16], and for studying the mechanobiological properties of ECM in BC [17,18]. Gelatin is derived from denatured collagen, after its partial hydrolysis, and its addition to 3D models can improve cell biocompatibility and proliferation [19]. Furthermore, gelatin hydrogels can replicate the tumor stiffness, thus altering the genotype and phenotype of BCCs [20]. Alginate is a biocompatible polysaccharide that can modify the mechanical properties of the models [21]. Due to its limited cell-adhesive properties, it is frequently combined with additional biomaterials, such as collagen and gelatin, to fabricate 3D-printed BC models that closely mimic the physiological characteristics of tumors *in vivo* [22,23].

The main objective of this work was to develop a 3D *in vitro* model of BC that reproduces the ECM properties found within tumors to recreate BCC malignancy and drug resistance occurring *in vivo*. For this purpose, MCF-7 cells were selected as the representative BCC line. The TME was mimicked using core-shell hydrogel beads composed of gelatin, alginate, and Col1. The hydrogel bead shell, composed of alginate, serves to spatially confine the proliferation of BCCs within the core as it occurs in the DCIS, where BCC growth occurs within the ducts, which are enclosed by a capsule formed by myoepithelial cells and the basement membrane [24]. Therefore, the shell in our model is designed to replicate this spatial constraint. In addition, the presence of the shell enables the maintenance of the core integrity, preventing gelatin leakage. Also, the incorporation of Col1 into the core of these artificial tumors enables the replication of the stiffness and high Col1 content found in breast tumors. Indeed, Col1 can enhance the malignant behavior of BCCs, thereby increasing the physiological relevance of the models for *in vitro* studies. To assess the similarities in behavior with *in vivo* tumors, we evaluated the stiffness and porosity of the designed prototypes, along with the proliferation, morphology, and expression of invasion, malignancy, and drug resistance markers in the BCCs embedded within the cancer models. Designed breast cancer models could provide a valuable platform for evaluating drug efficacy, given their ability to mimic the TME. Moreover, they could be well-suited for high-throughput screening of antitumor and chemotherapeutic agents.

2. Materials and methods

2.1. Materials

Alginate sodium salt from brown algae (Ref. 71,238), calcium chloride ($CaCl_2$), 4′,6-diamino-2-phenylindole, dihydrochloride (DAPI), dimethyl sulfoxide (DMSO), doxorubicin, and EDTA were purchased from Sigma Aldrich (Saint Louis, MO, USA). Gelatin (Quali-Pure 300P) from porcine skin was acquired from Rousselot (Gent, Belgium). Antibiotic-Antimycotic solution (Ref. 15,240,062), N-(2-hydroxyethyl) piperazine-N′-(2-ethanesulfonic acid) (HEPES), 2-mercaptoethanol, Dulbecco's phosphate-buffered saline (DPBS) 10× without Ca^{2+} and Mg^{2+}, Advanced Dulbecco's modified Eagle's medium (Advanced DMEM, Ref. 12,491,023), phosphate-buffered saline (PBS) without Ca^{2+} and Mg^{2+}, fetal bovine serum (FBS, Ref. 10,270,106), L-glutamine (Ref. 25,030,081), paraformaldehyde 4 %, were purchased in Thermo Fisher Scientific (Waltham, MA, USA). Acti-stain 488 phalloidin was purchased from Cytoskeleton (Denver, CO, USA). OptiCol Rat Collagen Type I was acquired in Cell Guidance Systems (Catalog No. MS18, Cambridge, United Kingdom). Goat serum, anti-Ki67 antibody (ab16667), and Alexa Fluor 647 goat anti-rabbit IgG H&L (ab150079) were purchased from Abcam (Cambridge, UK).

2.2. Cell culture

MCF-7 (HTB-22, ATCC) cells were cultured in Advanced DMEM medium supplemented with 10 % FBS, 1 % Antibiotic-Antimycotic solution, and 1 % L-glutamine.

2.3. Biofabrication of core-shell hydrogel beads

Core-shell hydrogel beads with an alginate shell and a core composed of Col1, alginate, and gelatin were prepared to support cell encapsulation and culture. Core and shell pre-gels were formulated under sterile conditions. Col1 was extracted from rat tail tendons following established protocols [25], and its concentration was determined by microBCA assay (Ref. 23,235, Thermo Fisher Scientific), using OptiCol Rat Collagen Type I as a standard. The extracted Col1 was neutralized with 1 M NaOH, and its osmolarity was adjusted with 10× DPBS. Alginate (2.5 %) was dissolved in PBS and stirred overnight at room temperature (RT), while gelatin (20 %) was dispersed in PBS and incubated at 37 °C overnight. Pre-gels were prepared by mixing the components according to the formulations specified in Table 1, and the final volume was adjusted with cell culture medium. MCF-7 cells were incorporated into the hydrogel core by spinning 1.5×10^7 cells (300 g, 4 min) and resuspending the pellet in 3 mL of core pre-gel using a positive displacement pipette.

Core-shell hydrogel beads were fabricated using a coaxial needle system, with controlled flow rates of the shell and core pre-gels. The produced prototypes were subsequently introduced into a 50 mM $CaCl_2$ in 10 mM HEPES solution under stirring, where they were crosslinked for 10 min. After crosslinking, the core-shell hydrogel beads were washed with PBS and individually transferred into wells of a 48-well plate. Then, 0.5 mL of culture medium was added to each well, and they were incubated at 37 °C in the cell incubator. For comparison, two control groups were included: Col1 hydrogels at 4 mg/mL and MCF-7

Table 1
Composition of the prototypes of the core-shell hydrogel beads. The prototypes were described in the following format: GXAXCX, where X represents the concentration in % (*w/v*) of gelatine (G), alginate (A), and Col1 (C) constituting the core of the hydrogel.

Prototypes	Core			Shell	Crosslinking	Cell density	Young's Modulus
	Gelatin	Alginate	Col1	Alginate			
G3A1	3 %	1 %	–	2.5 %	$CaCl_2$	$5{\cdot}10^6$cells/mL	2.280 ± 0.524 KPa
G3A0.5	3 %	0.5 %	–	2.5 %	$CaCl_2$	$5{\cdot}10^6$cells/mL	2.072 ± 0.200 KPa
G3A1C0.4	3 %	1 %	0.4 %	2.5 %	37 °C + $CaCl_2$	$5{\cdot}10^6$cells/mL	2.411 ± 0.206 KPa
G3A0.5C0.4	3 %	0.5 %	0.4 %	2.5 %	37 °C + $CaCl_2$	$5{\cdot}10^6$cells/mL	2.122 ± 0.094 KPa

cells cultured in a standard 2D monolayer. The Col1 controls were prepared by embedding 5×10^6 cells/mL into 25 μL hydrogels of 0.4 % Col1, while the 2D model involved direct seeding of cells onto multi-well plates.

2.4. Evaluation of hydrogel mechanical properties and porosity

2.4.1. Mechanical properties

The Young's modulus of the hydrogels was measured using compression testing, with core-shell hydrogel beads to assess the overall system stiffness and disc-shaped hydrogels to evaluate the stiffness of the core hydrogel embedding BCCs. Core-shell hydrogel beads were prepared as described before (section 2.3), without the cell addition, whereas hydrogel discs were prepared in 48-well plates, with 400 μL of each of the pre-gels forming the core of the beads.

The measurements were conducted using a TA.XT.plus Texture Analyzer (Stable Micro Systems) equipped with a 5 kg load cell. Compression tests were performed at room temperature, applying a force of 1 N at a speed of 1 mm/s using 3 experimental replicates ($n = 3$). The results were obtained using the Texture Exponent 32 V 6.1.12.0 software. For hydrogels with a disc shape (n = 3), the Young's modulus was calculated by determining the slope of the stress/strain curves in the linear range. For the core-shell hydrogel beads, the Young's modulus was calculated using the Hertz equation (Eq. 1), where F is the force applied, G is the elastic modulus, and ΔD is the difference between the initial undeformed diameter (D) and the deformed diameter of the gel sample.

$$F = \frac{4}{3} \cdot G \cdot D^{0.5} \cdot \Delta D^{1.5} \quad (1)$$

2.4.2. Porosity

The porosity of the core-shell hydrogel beads was also evaluated by Scanning Electron Microscopy (SEM, ZEISS FESEM Ultra Plus, Zeiss) using 3 experimental replicates ($n = 3$). Beads were freeze-dried at a condenser temperature of −70 °C and a vacuum of 0.1 mBar for 48 h (Telstar LyoQuest HT40). The freeze-dried beads were then sliced in half with a scalpel and sputter-coated with 10.0 nm of iridium (Quorum Q150T-S-Plus, Quorum Technologies).

2.5. Assessment of cell proliferation, metabolism, and drug efficacy

2.5.1. Cell proliferation and metabolism

Cell proliferation and metabolic activity within the cell-laden core-shell hydrogel beads (hydrogels containing cells encapsulated in the core) were assessed utilizing AlamarBlue (Thermo Fisher Scientific). On days 1, 2, 4, 7, and 9, the cell medium was replaced with a 10 % solution of AlamarBlue in the cell medium. Following a 1-h incubation period within the 37 °C incubator (time that has been previously used for hydrogels with high cell density [26]), media samples from each hydrogel were extracted and analyzed for fluorescence emission (560/590 nm). Eight experimental replicates were employed for each experimental condition ($n = 8$). The cellular proliferation was also analyzed by determining the double-stranded DNA (dsDNA) using Quant-iT PicoGreen assays (Thermo Fisher Scientific). At different time points, cell-laden hydrogels ($N = 4$) were recollected into 0.5 mL of TE buffer, and hydrogels were disrupted by three cycles of freezing and thawing, followed by mechanical fragmentation using an up-and-down motion through a syringe. Then, dsDNA was quantified according to the manufacturer's protocol.

2.5.2. Drug efficacy

Drug efficacy against MCF-7 cells was also assessed after a week of maturation. Cell-laden hydrogels were incubated for one week to ensure cell growth and then exposed to differing concentrations of doxorubicin for 48 h. Following incubation, cellular viability was assessed using the AlamarBlue assay, employing the previously described methodologies. Hydrogels incubated with cell medium were utilized as negative controls. IC50 values were determined using GraphPad Prism 8.0 software (GraphPad Software). 5–6 experimental replicates were used per condition ($n_{G3A1} = 5$, $n_{G3A0.5,G3A1C0.4,G3A0.5C0.4,Col1,2D} = 6$).

2.6. Cell morphology examination

Cell morphology was examined by staining of the cell nuclei and cytoskeleton after 7 days in culture *via* confocal microscopy (Leica Stellaris, Leica Microsystems). Cell-laden hydrogels were washed twice with PBS, fixed with 4 % paraformaldehyde (20 min, RT), and permeabilized with 0.1 % Triton X-100 (5 min, RT). Then, hydrogels were blocked with 3 % BSA in PBS-Glycine 0.1 M (1 h, RT), incubated with Acti-stain 488 phalloidin (3.5:500, 45 min, RT), and followed by DAPI (1: 500, 10 min, RT). Three washes with 3 % BSA in PBS were performed between steps. The analysis of spheroid quantity and size was conducted using FIJI software [27]. The number of spheroids quantified in each prototype ($N = 3$) was above 900 (Col1:2442, G3A1: 1734, G3A0.5: 962 G3A1C0.4: 2762, G3A0.5C0.4: 3355).

2.7. Immunofluorescence

Expression of Ki67 was assessed in the cell-laden hydrogels by immunofluorescence using a confocal microscope ($N = 2$) (Leica Stellaris, Leica Microsystems). Cell-laden hydrogel samples were collected, fixed, and permeabilized at day 7, as explained in section 2.6. Next, hydrogels were incubated with the blocking solution (3 % BSA in PBS-Glycine 0.1 M-Tween-20 0.1 % containing 10 % goat serum, 1 h, 4 °C). Then, they were incubated with an anti-Ki67 antibody (1:250, 4 °C, overnight), with goat antirabbit IgG H&L (1:500) and Acti-stain 488 phalloidin (1:350) (4 °C, 2 h), and with DAPI (1:500, 4 °C, 10 min), all of them in the blocking solution. After each step, three washes with the blocking solution were performed.

2.8. RNA isolation and RT-qPCR

The differences in the gene expression between prototypes were analyzed by RT-qPCRs and compared with Col1 and 2D controls. After 7 days of incubation, cell-laden hydrogels were collected and washed with PBS. Four capsules were used per biological replicate. They were stored at −80 °C in RLT lysis buffer containing 1 % β-mercaptoethanol until RNA isolation. For RNA isolation, hydrogels were physically disrupted with a needle and syringe as specified in section 2.5. The collected cell

lysate supernatant was subsequently used for RNA isolation, using the *RNeasy Plus Mini Kit* (Qiagen) according to the manufacturer's instructions. The amount of RNA in each hydrogel was measured with a UV/Vis nano spectrophotometer (Nabi, Microdigital). Then, a two-step RT-qPCR was performed. cDNA from the isolated RNA was synthesized using the *iScript cDNA Synthesis Kit* (BIO-RAD). Then, the gene expression was analyzed by RT-qPCR of all cDNA samples (1.5 ng), using the *iTaq Universal SYBR Green Supermix* (BIO-RAD) and the corresponding primer (500 nM, Table S1, Sigma Aldrich). The protocol followed for the QuantStudio 3 (Applied Biosystems) was 1 cycle of polymerase activation and DNA denaturation at 95 °C for 10 min, 40 cycles of annealing and extension, consisting of 15 s at 95 °C and 1 min at 60 °C, and the melt curve analysis was performed. The $2^{-\Delta\Delta Ct}$ method was employed to determine the fold change in gene expression, using the 18S ribosomal RNA as a housekeeping gene due to its stability as a reference gene in eukaryotic cells [28]. RT-qPCRs were performed in triplicate ($N = 3$).

2.9. Statistical analysis

The data represent the mean value and the standard deviation, and the number of experimental replicates (n) or biological replicates (N) is specified in each section. Statistical analysis was carried out with the GraphPad Prism 8.0 software (GraphPad Software). To determine statistically significant differences between prototypes, one-way, and two-way ANOVAs were conducted ($\alpha = 0.05$). A *p*-value threshold of less than 0.05 was used to define statistical significance.

3. Results and discussion

3.1. Core-shell hydrogel beads preparation and characterization

Core-shell hydrogels allow the formation of cancer models consisting of a tumor core and an outer stromal layer, which enables the replication of the tumor anatomy [29]. The hydrogels' core can be tuned to provide an ECM-like environment that allows the formation of cancer tumoroids within the core to replicate the malignancy of human tumors. Therefore, these hydrogels facilitate the study of cell interactions and behavior in a confined 3D environment. Furthermore, the alginate shell provides the necessary mechanical stability and porosity to maintain the structure of the hydrogels, prevent cell proliferation outside the bead, and enable the diffusion of nutrients and oxygen [30]. Moreover, the outer layer could also be tuned to allow the inclusion of stromal cells to replicate the tumor anatomy. Core-shell hydrogels have significant potential for cancer modeling and drug screening, primarily due to their ability to support spheroid development within their interior [31–33].

Core-shell hydrogel beads with a 2.5 % alginate shell were developed, while the core composition was systematically varied to explore different microenvironment conditions (Scheme 1). The cores consisted of gelatin (3 %) combined with alginate (0.5–1 %) and Col1 (0–0.4 %), with the alginate concentration adjusted to modulate stiffness, given its known role in promoting proliferation and survival pathways [34]. The impact of Col1 incorporation was also investigated, considering its relevance to breast cancer cell (BCC) behavior. For clarity, the different core-shell hydrogel prototypes are referred to according to their core compositions (G3A1, G3A0.5, G3A1C0.4, G3A0.5C0.4), as summarized in Table 1. All experimental outcomes were compared with results from Col1 hydrogel and 2D culture control models.

To avoid blocking or problems with the homogeneity of the hydrogels, the shell pre-gels were maintained at RT, whereas the core pre-gels were prepared just before their use. To do so, gelatin-alginate dispersions were incubated at 37 °C, and mixed with Col1 (only in G3A1C0.4 and G3A0.5C0.4) and cells just before the extrusion to reduce the gelatin viscosity, the crosslinking of Col1, and problems in cell distribution. To facilitate hydrogel coagulation, the core-shell hydrogel beads were incubated under stirring in a refrigerated 50 mM $CaCl_2$ solution in 10 mM HEPES. This process improved the coagulation of gelatin in the core and prevented its collapse within the shell. This method of fabrication renders core-shell hydrogel beads of 2.6–2.9 mm in diameter (G3A1: 2.887 ± 0.024 mm; G3A0.5: 2.750 ± 0.132 mm; G3A1C0.4: 2.577 ± 0.079 mm; G3A0.5C0.4: 2.703 ± 0.052 mm).

To ensure that the core-shell hydrogel beads closely replicate the tumor stiffness, the mechanical properties of the beads and the core were evaluated. The Young's modulus of the whole core-shell hydrogel bead was approximately 2.2 KPa (Table 1), with no significant differences observed between prototypes despite variations in their core composition (Fig. 1A). The lack of statistically significant differences between Young's modulus values across the core-shell hydrogel beads could be attributed to the consistent presence of 2.5 % alginate in the shell, which regulates the total bead stiffness. To investigate the mechanical effects of the different core compositions on MCF-7 cells, disc-shaped hydrogels of gelatin, alginate and Col1 with identical pre-gel composition to that of the beads' core were designed, and their Young's modulus was measured (Fig. 1B). Prototypes G3A1 and G3A0.5

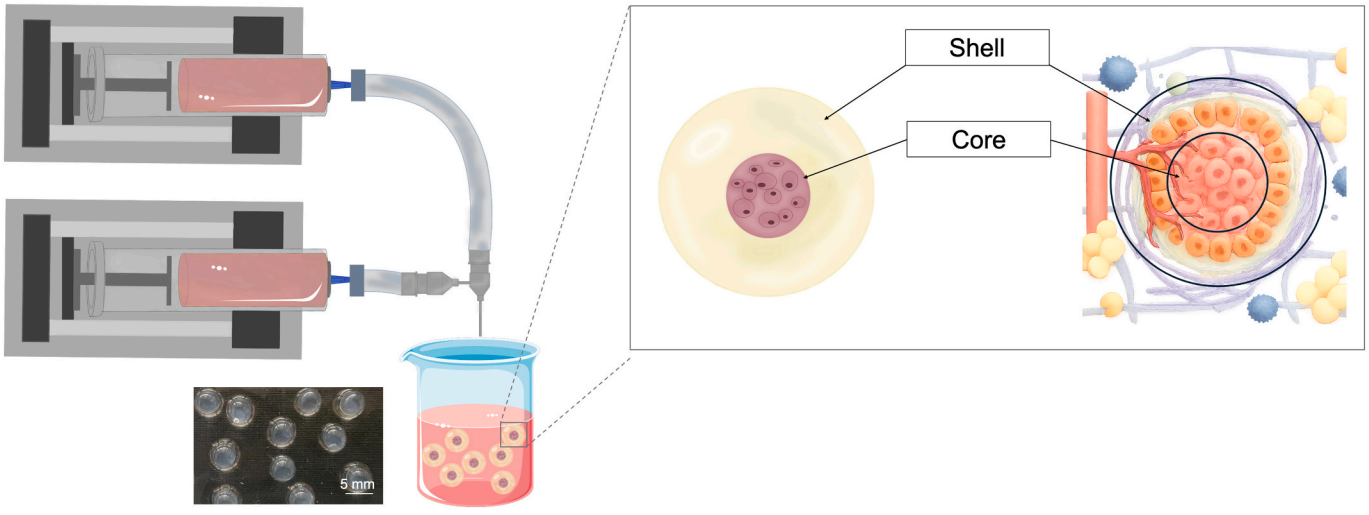

Scheme 1. Schematic representation of the core-shell hydrogel bead preparation process at room temperature and model of ductal carcinoma *in situ* recreation. The diagram illustrates the structural similarities of the core–shell hydrogel beads and the tumor. The tumor microenvironment representation was created with Illustrae.co.

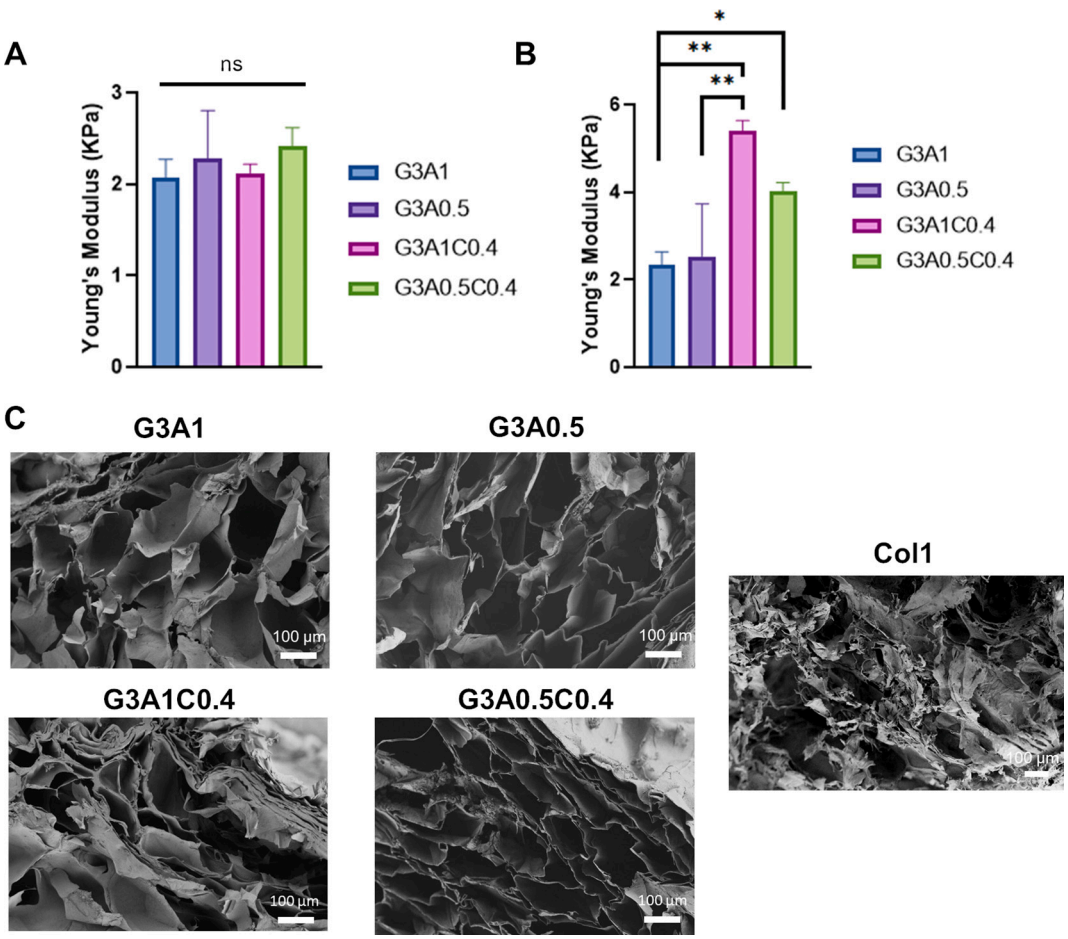

Fig. 1. Hydrogel mechanical properties and porosity. (A) Young's Modulus of the whole prototypes G3A1, G3A0.5, G3A1C0.4, G3A0.5C0.4 (One-way ANOVA, $n = 3$). (B) Young's modulus of the core of prototypes G3A1, G3A0.5, G3A1C0.4, G3A0.5C0.4 (One-way ANOVA, n = 3, ns: no significant, *: $p < 0.05$, **: $p < 0.01$). (C) Images of the hydrogels' porosity by Scanning Electron Microscopy of Col1, G3A1, G3A0.5, G3A1C0.4, G3A0.5C0.4 (n = 3). Scale bar 100 µm.

had lower Young's modulus (G3A1: 2.534 ± 1.198 KPa; G3A0.5: 2.331 ± 0.307 KPa) than the prototypes containing Col1 (G3A1C0.4: 5.404 ± 0.229 KPa; G3A0.5C0.4: 4.014 ± 0.203 KPa), being only statistically significant in the case of the higher content of alginate (G3A1 *vs* G3A1C0.4: $p < 0.05$), probably due to the higher variability in the hydrogels with lower alginate content. Nevertheless, the addition of Col1 increases the stiffness of the core, enabling the replication of the stiffness of breast tumors *in vivo* (2.2–5 KPa) [35,36]. Moreover, a synergistic effect was observed between higher concentrations of alginate and the presence of Col1, as evidenced by the higher Young's modulus of the core of G3A1C0.4 compared to G3A0.5C0.4, in agreement with previous reports [37,38].

The porosity of the hydrogels was examined using scanning electron microscopy (SEM, Fig. 1C). All prototypes exhibited large pores, with no discernible differences between them or between the core and shell, and similar to other alginate/gelatin-based hydrogels [39], suggesting that nutrients and drugs could diffuse into the core-shell hydrogels. No fibrous structure attributed to Col1/gelatin could be detected, which could be caused by artifacts created during the freeze-drying process. Since the porosity remained stable across all prototypes, any differences in the biological properties of the hydrogels cannot be attributed to variations in the number or size of pores, and must be dependent on the hydrogel composition and stiffness.

3.2. Proliferation and metabolic activity

The incorporation of Col1 in hydrogels has already shown an increase in the metabolic activity of BCCs [40,41]. The Col1 present in the tumor ECM contributes to the structure, stiffness, and hypoxia of the TME observed *in vivo*. These elements, along with Col1 interactions, play an important role in tumor metabolism by activating key metabolic and survival pathways, such as PI3K and Akt [5,41]. Thus, we explored whether the introduction of Col1 in the developed core-shell hydrogel beads could have any effect on BCCs.

The metabolic activity of BCCs in the core-shell hydrogel beads was analyzed by AlamarBlue at different time points of incubation, and compared with cells growing in 2D and Col1 hydrogels (Fig. 2A). Despite the lower metabolic activity (fluorescence values) of hydrogels containing Col1 (G3A1C0.4, G3A0.5C0.4) than hydrogels without Col1 (G3A1, G3A0.5) at day 2, there were no significant differences between the prototypes after 4 days in culture. Nevertheless, 2D and Col1 controls consistently exhibited the highest fluorescence values across all measured days. However, the differences between the initial cell number per prototype and controls could be responsible for the differences observed. Variations in pre-gel viscosity result in different levels of stress on the cells during encapsulation, leading to sample-dependent changes in cell viability. To account for this, the metabolic activity fluorescence data for each sample were normalized to their respective day 1 values (Fig. 2B). The core-shell hydrogel beads (G3A1C0.4, G3A0.5C0.4, and G3A0.5) and Col1 exhibited higher metabolic activity rates when normalized to day 1 in comparison with 2D. This is mainly because cells growing in 2D reached confluency on day 2 and began to detach from the wells and form cell sheets. Cells growing in G3A1 exhibited the lowest cell metabolism activity compared to the other prototypes,

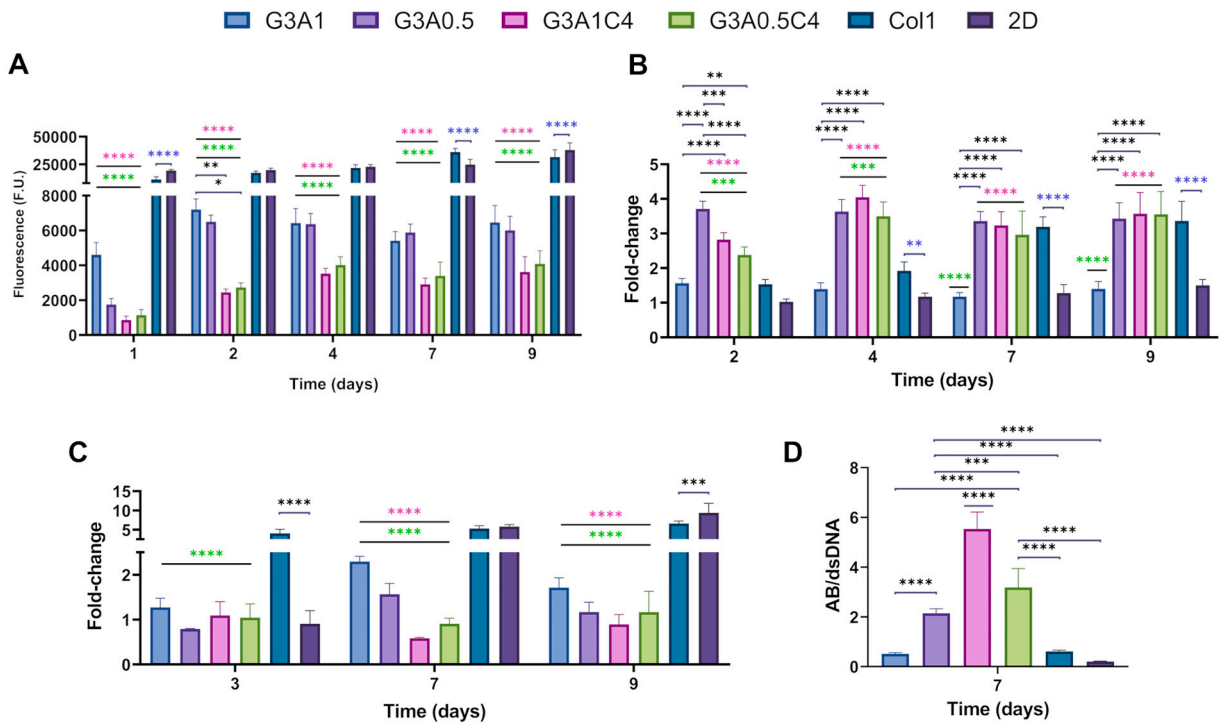

Fig. 2. MCF-7 proliferation and metabolism activity on the core-shell hydrogel beads. (A) MCF-7 metabolism activity by AlamarBlue Assay. Results are presented in fluorescence units (Two-way ANOVA, $n = 8$). (B) MCF-7 metabolism activity by AlamarBlue Assay. Results are normalized by day 1 (Two-way ANOVA, n = 8). (C) MCF-7 double-stranded DNA quantification by PicoGreen. Results are normalized by day 1 (Two-way ANOVA, $N = 4$). (D) MCF-7 metabolic rates by comparing AlamarBlue and PicoGreen (One-way ANOVA, n = 8) (*: $p < 0.05$, **: $p < 0.01$, ***: $p < 0.001$, ****: $p < 0.0001$; pink asterisks: core-shell models *vs* 2D, green asterisks: core-shell models *vs* Col1, blue asterisks: Col1 *vs* 2D, black asterisks: Differences between core-shell models). (For interpretation of the references to colour in this figure legend, the reader is referred to the web version of this article.)

indicating that this core composition did not promote cell metabolism. Furthermore, G3A0.5 did not promote the increase in metabolic activity over time. In contrast, the presence of Col1 provoked an increase in the cell metabolic activity over time, similar to Col1 controls, but no differences were observed between G3A0.5, G3A1C0.4, and G3A0.5C0.4 on days 4, 7, and 9.

To determine whether the differences observed between conditions were linked to an increase in the cell number or an increase in the metabolic activity, the dsDNA content in each prototype was quantified at different time points. As expected, Col1 and 2D controls exhibited higher dsDNA content compared to the prototypes, and no differences were observed between the core-shell hydrogel beads (Fig. 2C), indicating that cell proliferation occurred to a similar extent. To evaluate if MCF-7 cells had a higher metabolic activity in the core-shell hydrogel beads due to the Col1 presence, the fluorescence values of AlamarBlue were normalized with the dsDNA values (both normalized by day 1, Fig. 2D). At day 7, prototypes G3A0.5, G3A1C0.4, and G3A0.5C0.4 had statistically significantly higher metabolic rates than 2D and Col1. Specifically, G3A1C0.4 exhibited the highest metabolic activity, attributed to the stiffness of the pre-gel in which the cells are embedded, and the activation of metabolic pathways mediated by the presence of Col1. Previous studies have already shown the role of collagen in ECM remodulation and the TME. Crosslinking collagen fibers regulates matrix stiffness, promoting cell adhesion *via* integrin activation, cell proliferation and survival *via* PI3K/AKT pathway, and tumor invasiveness and metastasis [34,41]. As observed previously, G3A1 demonstrated lower metabolic activity, similar to Col1 and 2D.

To confirm our results, we assessed the expression of Ki67 (Fig. 3A) and glyceraldehyde-3-phosphate dehydrogenase (GAPDH, Fig. 3B). Ki67 is a proliferation-related gene, and its high expression is linked with microinvasion and higher-grade lesions in BC [42]. Prototypes containing Col1 showed an upregulation of this gene; prototype G3A1C0.4 exhibited higher Ki67 expression compared to the other prototypes. To determine whether the overexpression of Ki67 observed at the RNA level in G3A1C0.4 and G3A0.5C0.4 is also reflected at the protein level, immunofluorescence imaging was performed using confocal microscopy (Fig. 3C). MCF-7 cells formed spheroids with a high Ki67 expression in all prototypes, confirming the high proliferative activity across the models. The differences observed at the RNA level may be associated with the reduced proliferation detected by PicoGreen in G3A1 and G3A0.5 after 7 days, which corresponds to the time point at which RT-qPCR samples were collected. GADPH is also linked with cell metabolic activity, as this enzyme participates in glycolysis [28]. Again, prototypes with Col1 in the core showed an upregulation of this gene in the RT-qPCR studies, although it was not statistically significant. All these results together indicated that the incorporation of Col1 into the hydrogel core (prototypes G3A1C0.4 and G3A0.5C0.4) could reprogram the BCCs to exhibit a higher metabolic activity.

3.3. MCF-7 morphology

The cell morphology was assessed using confocal microscopy with a staining of the cell nuclei and cytoskeleton. By day 7, BCCs formed small spheroids and cell aggregates in the cores of all prototypes (Fig. 3D-E). However, variations in spheroid size and number were noted. Specifically, prototypes containing Col1 in the core exhibited smaller spheroids, often surrounded by single cells (Fig. 3F, G3A1C0.4: 386.80 μm^2, G3A0.5C0.4: 565.76 μm^2). The spheroids embedded in the prototypes without Col1 showed the highest area (G3A1: 1308.87 μm^2, G3A0.5: 1077.19 μm^2), similar to Col1 controls (975.97 μm^2). These results could be related to the higher stiffness produced by the core of the prototypes with Col1 (Fig. 1B), since it has been reported that MCF-7 cells form smaller spheroids in stiffer gels than in soft gels [43,44].

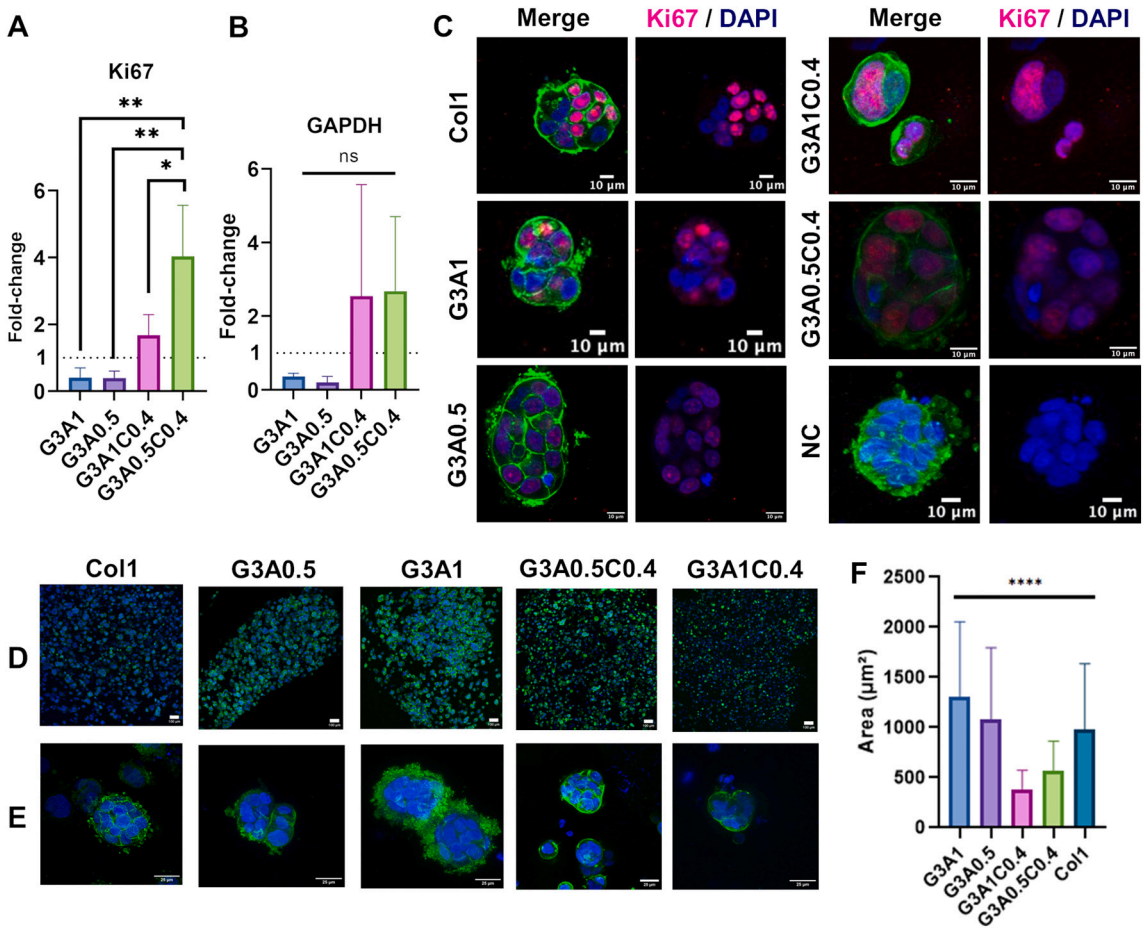

Fig. 3. MCF-7 proliferation, metabolic markers expression, and cell morphology in the core-shell hydrogel beads G3A1, G3A1C0.4, G3A0.5, and G3A0.5C0.4 for 7 days. (A-B) Expression of the gene Ki67 (A), associated with cell proliferation, and GADPH (B), associated with cell metabolism. $2^{-\Delta\Delta Ct}$ values were calculated with the ΔCt from Col1 cultures (One-Way ANOVA, $N = 3$, ns: no significant, *: $p < 0.05$, **: $p < 0.01$). (C) Expression of Ki67 (pink) by immunofluorescence in the core-shell hydrogel beads and Col1 controls ($N = 2$). The cell cytoskeleton was stained with Acti-stain 488 phalloidin (green), and cell nuclei with DAPI (blue). Scale of 10 µm. A negative control stained with only the secondary antibody was also performed to ensure that there was no non-specific binding. (D) MCF-7 morphology and organization across the hydrogels Col1, G3A0.5, G3A1, G3A0.5C0.4, and G3A1C0.4. Cells were stained with Acti-stain 488 phalloidin (green) and DAPI (blue) at day 7. Scale of 100 µm (One-way ANOVA, $N = 3$). (E) Close-up image of MCF-7 spheroids in Col1, G3A0.5, G3A1, G3A0.5C0.4, and G3A1C0.4. Scale of 25 µm. (F) Area of the spheroids (µm^2) embedded in G31, G3A0.5, G3A1C0.4, G3A0.5C0.4, and Col1 (One-way ANOVA, N = 3, ****: $p < 0.0001$). (For interpretation of the references to colour in this figure legend, the reader is referred to the web version of this article.)

3.4. MCF-7 invasiveness

As F-actin structures were observed on the spheroid surface in Col1, G3A0.5, and G3A1 prototypes (Fig. 3D-E), we hypothesize that these protrusions could be related to invadopodia. This phenomenon is characterized by protrusions in the cell membrane rich in actin, which are associated with cell invasiveness, as they are involved in the degradation of the ECM to promote cell invasion [45–47]. Despite MCF-7 cells exhibiting low basal invasiveness, these cells can modulate their plasticity in response to interactions with the surrounding microenvironment. Therefore, previous studies have shown that, under 3D culture conditions and in the presence of suitable biomaterials, such as collagen, MCF-7 cells can alter their metabolic and genetic profiles to enhance invasive potential [48,49]. Given the F-actin structures observed in the morphological cell studies of the core-shell hydrogel beads, we evaluated invadopodia-related markers by RT-qPCR (Fig. 4) to determine if these structures were associated with invasion. First, the expression of HIF1α and CSRP2 was evaluated. Breast tumors can experience hypoxia, which activates gene pathways that facilitate proliferation and invasion [50]. The absence of oxygen induces the activation of HIF1α, which subsequently activates the transcription of related genes, such as CSRP2, which organizes actin filaments to support the formation of invadopodia [45]. Prototypes containing Col1 in the core showed the highest expression of HIF1α, whereas the prototypes containing 1 % alginate in the core (G3A1 and G3A1C0.4) had the highest expression of CSRP2, being upregulated only in the case of G3A1C0.4 (G3A0.5 and G3A0.5C0.4 showed no expression of this gene, with Ct values above 35). Although these values were not statistically significant, the tendency towards a higher gene expression than the Col1 model suggests that hypoxia could be responsible for the appearance of the small invadosomes observed in G3A1C0.4, but not in G3A1 or G3A0.5, where larger protrusions were observed. In addition, the higher stiffness of G3A1C0.4 could be related to the upregulation of CSRP2, as the degree of hypoxia is more pronounced and directly regulates the expression of CSRP2 [51]. These results indicate that hypoxia cannot be responsible for the F-actin protrusions observed in G3A1 and G3A0.5.

During invadopodia formation, an actin core develops from which actin filaments organize and extend, enabling the cell to drive forward and invade surrounding tissues. The creation of this structure is mediated by the coactivators N-WASP (WASL) and cortactin (CTTN) (Fig. 4) [45,47]. CTTN was downregulated in all designed prototypes compared to Col1, whereas N-WASP was modestly upregulated only in G3A1C0.4 and G3A0.5C0.4. We also analyzed the expression of F-actin (α-actin, β-actin, or γ-actin) in the prototypes to determine whether there was

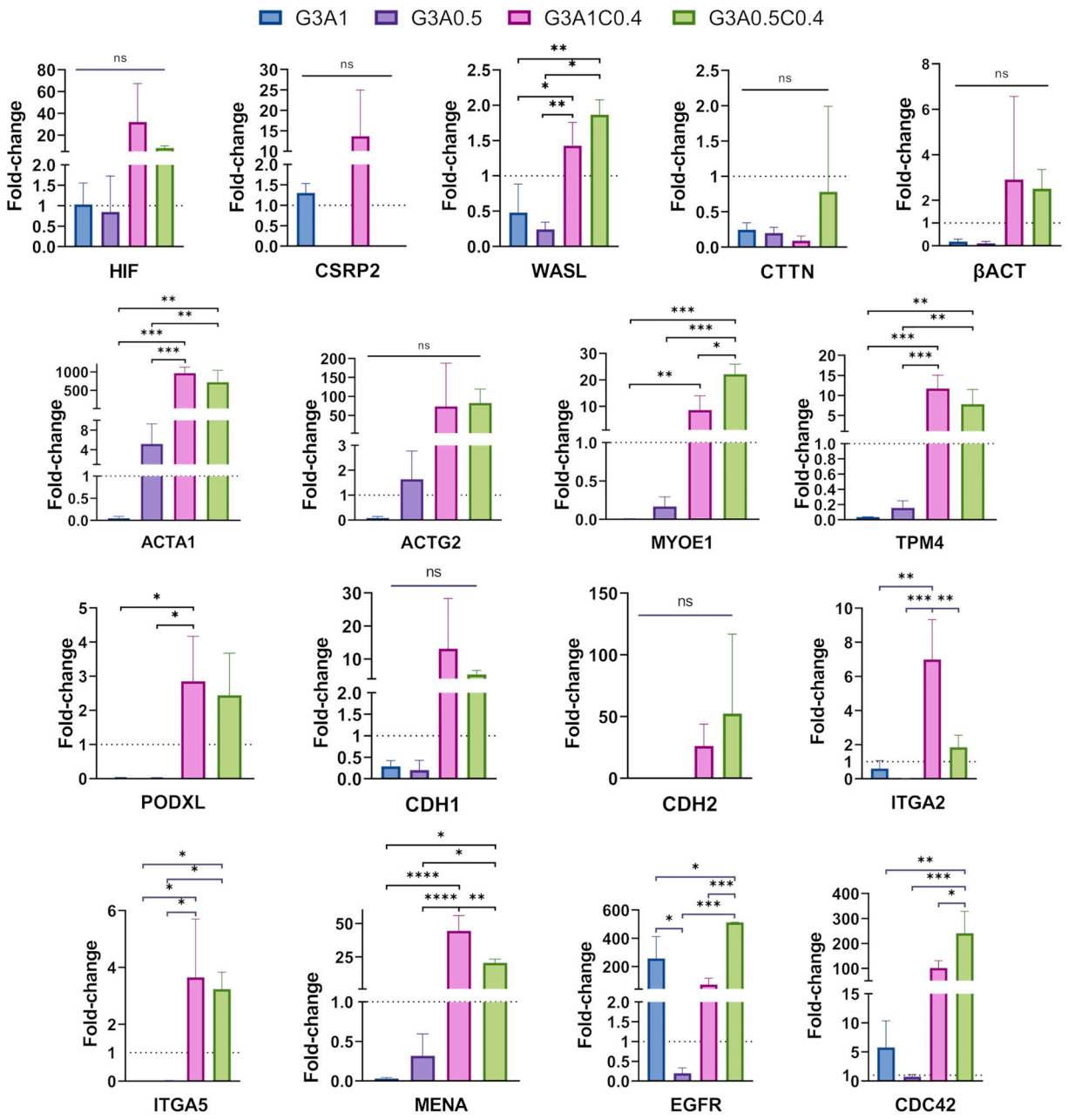

Fig. 4. Expression of invasiveness genes (HIF1α, CSRP2, WASL, CTTN, βACT, ACTA1, ACTG2, MYO1E, TPM4, PODXL, CDH1, CDH2, ITGA2, ITGA5 MENA, EGFR, CDC42) in MCF-7 grown in hydrogels G3A1, G3A1C0.4, G3A0.5, and G3A0.5C0.4 for 7 days. $2-\Delta\Delta Ct$ values were calculated with the ΔCts from Col1 cultures (One-way ANOVA, $N = 3$) (ns: not significant, *: $p < 0.05$, **: $p < 0.01$, ***: $p < 0.001$, ****: $p < 0.0001$).

upregulation of these genes that can explain the observed results (Fig. 4). Although G3A1C0.4 and G3A0.5C0.4 showed a modestly higher βACT expression level than Col1, there was no statistically significant difference between the prototypes. Additionally, G3A1C0.4 and G3A0.5C0.4 presented an upregulation of ACTA1 (encoding Actin alpha 1) and ACTG2 (encoding Actin gamma 2), they were only statistically significant in the case of ACTA1. These results indicated that there was no overexpression of any specific type of F-actin genes in the prototypes displaying the larger number of protrusions. Nevertheless, the higher expression observed in the models containing Col1 within the core compared to the Col1 model is a positive outcome, as it indicates their ability to better mimic the behavior of *in vivo* tumors. As these characteristics are involved in the promotion of oncogenesis, cell migration, and epithelial-to-mesenchymal transition (EMT) through pathways such as annexins, integrin signaling, and ERK-MAPK [52]. Moreover, we evaluated if there was an upregulation of matrix metalloproteinase 9 (MMP-9), which is often overexpressed in BC, and is also linked to the invadopodia [53,54]. None of the prototypes exhibited MMP-9 expression (Fig. S1).

The downregulation of all invadopodia-related genes in the RT-qPCR results indicates that the actin-rich structures observed by confocal microscopy in Col1, G3A0.5, and especially G3A1, are not related to invadopodia. Based on these results, the next step was to investigate if there was an activation of any other invasion process in these models. Therefore, we evaluated the expression of markers related to blebbing, filopodia, or cell polarization (Fig. 4). Blebbing involves the formation of circular membrane protrusions that expand and retract from the cytoplasm, a process implicated in cell invasion and metastasis in BC [55]. We assessed the expression of two genes involved with this process, MYO1E and TPM4. Myosin-Ie (encoded by MYO1E) is an actin-based

motor protein that plays a crucial role in bleb formation, as it is part of the protein network that supports blebs from the inside, whereas Tropomyosin 4 (encoded by TPM4) is an actin-binding protein that is recruited and colocalized with actin during bleb formation [56]. Both G3A0.5C0.4 and G3A1C0.4 overexpressed MYO1E and TPM4. Another hypothesis involved the polarization of MCF-7 cells, leading to the formation of microvilli and surface extensions. Podocalyxin (PODXL) regulates this process by initiating the development of microvilli and recruiting F-actin. Indeed, PODXL expression is associated with a more aggressive tumor prognosis due to the increased invasiveness of these cells [57,58]. However, there was only an overexpression of PODXL in G3A1C0.4 and G3A0.5C0.4. We also evaluated the expression of MENA, which encodes a protein from the Ena/VASP family (ENAH) that regulates actin organization, promoting the formation of structures such as invadopodia, filopodia, or cell polarization. This protein plays a key role in controlling actin spike formation during the development of filopodia in BCCs [47,59]. Again, MENA was only overexpressed in the prototypes G3A0.5C0.4 and G3A1C0.4. Previous studies have shown that MENA expression is elevated when cells are cultured in stiffer environments, which is consistent with our observations in the prototypes containing Col1 in the core [60]. These results indicated that blebbing, filopodia, and cell polarization did not correlate with the structures observed in G3A1, G3A0.5, and Col1 by confocal microscopy. However, the addition of Col1 to the core can increase the invasiveness of the cancer cells, promoting the appearance of membrane structures such as invadopodia, blebbing, filopodia, and cell polarization. This confirms the role of collagen in tumor invasion and metastasis observed in previous studies [61].

The expression of Cadherins, the molecules responsible for cell-cell adhesion, was also studied (Fig. 4). As BCCs become more invasive, the expression of E-cadherin is often downregulated to facilitate tumor progression [62]. Despite not finding statistically significant values, we observed that in G3A1 and G3A0.5, CDH1 was downregulated, while in G3A0.5C0.4 and G3A1C0.4, this gene was upregulated (Fig. 4). The loss of CDH1 expression reduces cell-cell interactions, thereby facilitating cell dissemination through the ECM [47]. In confocal microscopy, we observed smaller and more compact spheroids in the hydrogel core-shell hydrogel beads with Col1 in the core, which could be related to the higher expression of CDH1 in these prototypes (Fig. 3D-E). Since CDH1 expression correlated with the morphology observed in the confocal microscopy images, we theorize that this result could be associated with the increased stiffness of the hydrogels. In contrast to CDH1, N-cadherin (CDH2) expression is up-regulated in BC, being associated with a more invasive and metastatic phenotype. The expression of CDH2 regulates the adhesion between BCCs and other types of cells, promoting tumor invasion [63]. CDH2 was overexpressed in G3A1C0.4 and G3A0.5C0.4, indicating that these prototypes presented a tendency towards a higher invasiveness profile (Fig. 4). The prototypes G3A1 and G3A0.5 exhibited no expression of CDH2.

We also assessed whether the absence of Col1 in the prototypes could reduce the focal adhesion with the hydrogel matrix, and this could be responsible for the structural features observed. In breast cancer, integrin adhesion receptors mediate interactions with the surrounding ECM, which are essential for tissue invasion during metastatic progression [64,65]. For this reason, we studied the expression of two types of integrins in our models, α2β1 and α5β1, by assessing the expression of their alpha subunits. The α2β1 has a high affinity for Col1, while α5β1 presents a higher affinity for fibronectin [66,67]. Both alpha subunit genes (ITGA2, ITGA5) were overexpressed in G3A1C0.4 and G3A0.5C0.4 (Fig. 4), a behavior typically observed *in vivo*, where they regulate invasion and proliferation [68]. In contrast, G3A1 and G3A0.5 exhibited a lower expression of these markers than the Col1 model. We hypothesize that, in these models, cells may not be effectively interacting with the surrounding matrix, which could lead to the formation of actin protrusions.

To further investigate the pathway that could be activated in our models to explain the higher invasive phenotype in the prototypes containing Col1, the expression of EGFR and CDC42 was investigated (Fig. 4). The epidermal growth factor receptor (EGFR) is typically overexpressed in BC, being involved in the tumor invasion, stemness, and proliferation [69]. EGFR can enhance BCCs' proliferation by activating downstream pathways such as PKC, JAK-STAT, and PI3K-Akt [70]. Also, it has an effect regulating the development of stemness and promoting the invasion in breast cancer through other pathways such as MAPK [71]. Moreover, recent studies have reported the role of EGFR in focal adhesion and integrin activation, enhancing the interaction of the BCCs with the TME [72]. This marker was overexpressed in G3A1C0.4, G3A0.5C0.4, and, interestingly, in G3A1. We hypothesize that these results could be related to the F-actin structures observed, especially in G3A1, since previous studies have already demonstrated that invasion and invadopodia formation in BC can be regulated by the EGFR-Src-Arg-cortactin pathway [73]. The Rho GTPase cell division control protein 42 homolog (CDC42) increases cell proliferation through the MAPK and p53 pathway. The overexpression of CDC42 is often mediated by cellular surface receptors such as EGFR [74]. Also, overexpression of CDC42 in BC is related to cell invasion and metastasis, promoting filopodia and invadopodia formation, and acts as a hallmark of EMT [75]. In our study, CDC42 was overexpressed in G3A1 and, especially, in G3A1C0.4, and G3A0.5C0.4. These results correlate with the observed in EGFR, indicating that a pathway involving both proteins, such as MAPK or AKT, could be activated in our models, inducing tumor progression and invasion [74,75].

Although these results do not provide a conclusive explanation for the actin-rich structures observed by confocal microscopy in G3A1, G3A0.5, and Col1, the downregulation of ITGA2, and ITGA5 and the upregulation of EGFR and CDC42 could be behind the formation of these structures in the case of G3A1. However, another hypothesis is that these actin structures may correspond to early stages of exosome secretion, a process known to be involved in cellular invasiveness and ECM remodeling [76]. In contrast, all invasion markers analyzed were overexpressed in G3A1C0.4 and G3A0.5C0.4. Therefore, the addition of Col1 to the core of the core-shell hydrogel beads enables the upregulation of genes related to cell invasion, thus modulating the plasticity of MCF-7 cells towards a more invasive phenotype.

3.5. MCF-7 malignancy

BCCs continually remodel the ECM to adapt its characteristics for tumor growth, such as stiffness and composition. BCCs alter their gene expression patterns to increase the expression of ECM components, thereby modifying the biochemical and mechanical characteristics of the matrix. These modifications alter cellular signaling pathways, promoting metastasis and drug resistance, or supporting angiogenesis [77]. Since ECM remodeling markers are important determinants of BC malignancy, we studied the expression of some of these genes in MCF-7 cells embedded in the designed hydrogel beads' core (Fig. 5). First, we evaluated the expression of the genes Col1A1 and FN1 encoding collagen 1A1 and fibronectin I, as they are BC markers associated with malignant tumor development. The deposition of these proteins induces changes in the ECM, providing structural support for BCCs and enhancing their proliferation, differentiation, and migration [12,41,78]. The addition of Col1 to the core resulted in increased Col1A1 expression (Fig. 5), G3A1C0.4 being the prototype with the highest expression of this gene, and the lack of expression of FN1 ($Ct > 35$). On the contrary, G3A1 and G3A0.5 exhibited a downregulation of both genes when compared to the Col1 model. Other ECM remodeling genes, such as HAS2 and LAMB1, were also evaluated. HAS2 is the most efficient isoform of the enzyme responsible for producing hyaluronic acid (HA), and the presence of HA in the ECM promotes proliferation and migration, making HAS2 expression a negative prognostic factor [79,80]. In addition, laminins are the most abundant non-collagenous proteins in the BC ECM, laminin subunit beta 1 (LAMB1) being a more accurate imitation

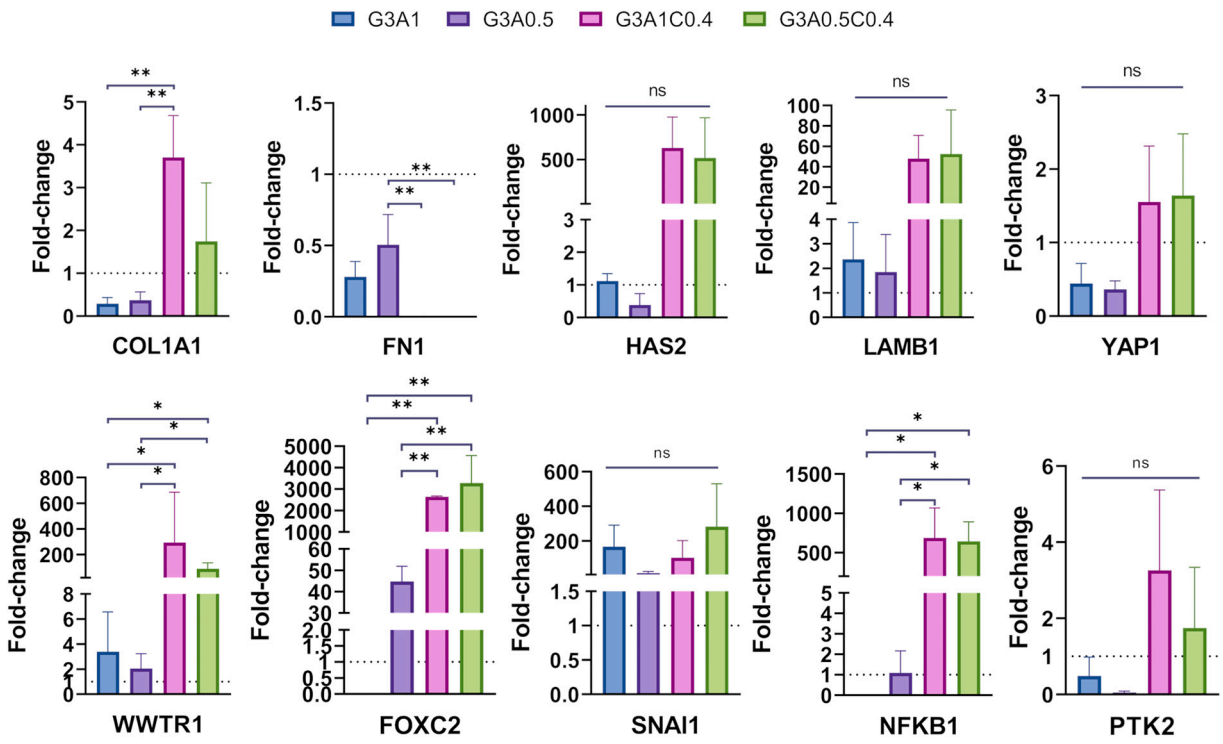

Fig. 5. Malignant tumor markers (Col1A1, FN1, HAS2, LAMB1, YAP1, WWTR1, FOXC2, SNAI1, NFKB1, PTK2) expression in MCF-7 grown in core-shell hydrogel beads G3A1, G3A0.5, G3A1C0.4, and G3A0.5C0.4 for 7 days. $2 - \Delta\Delta Ct$ values were calculated with the ΔCts from Col1 cultures (One-way ANOVA, $N = 3$, ns: not significant, *: $p < 0.05$, **: $p < 0.01$).

of the BC ECM and cell behavior [12]. G3A1C0.4 and G3A0.5C0.4 showed an upregulation of both genes (Fig. 5), whereas G3A1 and G3A0.5 showed an upregulation of LAMB1 and a downregulation of HAS2. Despite this tendency, there was no statistically significant difference between the prototypes. These results suggest that the incorporation of Col1 in the hydrogels tends to enhance the capability of BCCs to remodel the hydrogel matrix by depositing proteins present in the tumor ECM (Col1, HA, laminin) [12,81].

Mechano-sensing-related genes were also evaluated. YAP1 and WWTR1 (TAZ) are key effectors of the Hippo signaling pathway and are frequently overexpressed in BC, contributing to oncogenic processes [82,83]. These transcriptional coactivators modulate diverse cancer-related phenomena, including cell proliferation, invasion, drug resistance, EMT, and stemness, thereby promoting tumor development and progression [84–88]. The activation of YAP1 and WWTR1 is dependent on the high stiffness of the ECM in BC, and the expression of these coactivators is associated with increased cell proliferation [89]. Although all prototypes differed significantly from Col1, the expression of YAP1 and WWTR1 was higher in G3A1C0.4 and G3A0.5C0.4 (Fig. 4). As previously explained, the presence of Col1 in the core enhances stiffness, thereby activating the expression of YAP1 and WWTR1 in MCF-7 cells [90,91]. Furthermore, as mentioned before, various studies have linked the expression of these coactivators with cell transformations and tumor development in BC [89,92]. These findings suggest that G3A1C0.4 and G3A0.5C0.4 could serve as effective 3D BC models.

Finally, we also studied the expression of FOXC2, SNAI1, NFKB1, and PTK2, key BC genes associated with poor prognosis and with aggressive behavior (Fig. 5). FOXC2 is a transcription factor from the forkhead box family related to EMT and stemness pathways in BC [93,94]. Moreover, the expression of this marker has been associated with drug resistance, as it promotes the activation of pathways involved in ABC multidrug transport systems, prosurvival signaling cascades, and oxidative stress adaptation, thereby enhancing the proliferative potential of BCCs [95]. MCF-7 cells growing in G3A1C0.4 and G3A0.5C0.4 showed a statistically significant increase in this marker. SNAI1 is another transcription factor commonly overexpressed in BC, serving as a key marker of EMT and metastasis promotion [96,97]. In addition, SNAI1 contributes to immunosuppression, inhibition of apoptosis, and activation of protumorigenic signaling pathways [98]. Although the differences in SNAI1 expression between our models were not statistically significant, all designed models exhibited an overexpression of SNAI1 compared with the Col1 model, thereby better imitating the stemness and developmental characteristics of BCCs. We also analyzed nuclear factor kappa B1 (NFKB1), a key regulator of the proinflammatory environment characteristic of BC, which consequently promotes drug resistance, as well as the survival and proliferation of BCCs [99,100]. It is also involved in the development of EMT in breast cancer [101]. This marker exhibited a higher expression in the models containing Col1 in the core (G3A1C0.4, G3A0.5C0.4), indicating their ability to reproduce the EMT processes and cellular behavior observed *in vivo*. Lastly, we also studied the expression of the focal adhesion kinase (FAK), encoded by the gene PTK2. An increased expression of this marker in BC is often linked to metastasis, high cell survival, and proliferation [102]. Although no statistically significant differences were observed between the models, prototypes containing Col1 in the core showed a higher expression of this gene. This increased expression correlates with the results previously obtained for G3A1C0.4 and G3A0.5C0.4 when analyzing integrin subunit expression (ITGA2 and ITGA5), which is consistent with the known role of FAK as an adaptor molecule in integrin-mediated signaling pathways [103].

To investigate which mechanisms and pathways might be activated in the core-shell hydrogel beads containing Col1 in the core (G3A1C0.4 and G3A0.5C0.4), we analyzed the interactions between the proteins encoded by the overexpressed markers using a STRING interaction network (Fig. 6). Many overexpressed markers are related to the regulation of cell migration, promoting invasion to the surrounding matrix and metastasis of the BCCs (Fig. 6, light blue). Tumors increase their invasiveness by remodeling and stiffening the surrounding ECM and by engaging integrin-mediated and other signaling pathways that facilitate

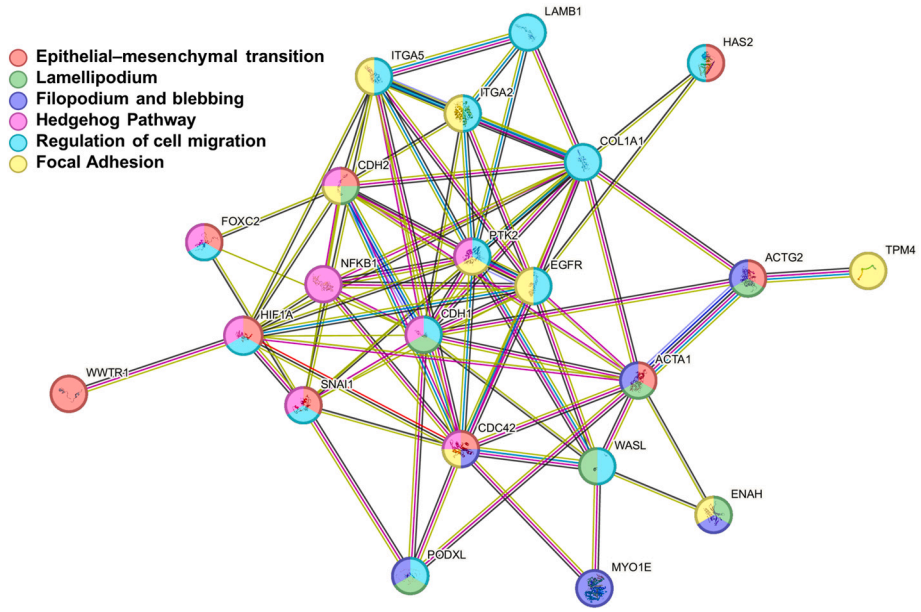

Fig. 6. STRING protein–protein interaction network for the 22 proteins whose genes were significantly overexpressed in the core-shell hydrogel beads containing Col1 in the core (G3A1C0.4 and G3A0.5C0.4). Nodes represent proteins, and edges indicate predicted or known interactions. Node colors correspond to the biological mechanisms or pathways in which the proteins are involved.

cell-ECM interactions [104]. As shown in the figure, many of the overexpressed markers are associated with focal adhesion (Fig. 6, yellow), highlighting the ability of BCCs embedded in these models to interact with their surrounding microenvironment. Additionally, invadopodia-related markers are upregulated in the presence of Col1, leading to the activation of lamellipodia, filopodia, and blebbing structures (Fig. 6, green and dark blue) in MCF-7 cells and, in consequence, enhancing their invasiveness potential [105]. Several of the identified markers and their encoded proteins are linked to the Hedgehog (Hh) signaling pathway (Fig. 6, pink), which is known to drive key processes in invasive BC, including proliferation, drug resistance, invasion, angiogenesis, and EMT [106–108]. We hypothesize that this pathway may be activated in our models, thereby enhancing their ability to replicate the behavior of *in vivo* tumors. Moreover, as previously discussed, several markers (Fig. 6, red) are also involved in promoting EMT, a hallmark process in BC through which cells acquire stem-like properties, enhancing their migratory capacity and chemoresistance [109]. This extensive network of protein interactions and pathway activations indicates that G3A1C0.4 and G3A0.5C0.4 could provide a more translatable model for breast cancer research.

3.6. Drug resistance

Finally, we studied the potential of the core-shell hydrogel prototypes developed as BC models for screening chemotherapeutic agents and other drugs. We compared the MCF-7 viability after incubating for 48 h with doxorubicin in G3A1, G3A0.5, G3A1C0.4, and G3A0.5C0.4 and Col1 and 2D controls. Doxorubicin was chosen as a drug model because of its efficacy and potency in the treatment of BC [110,111]. Core-shell hydrogels were incubated for 7 days before adding the different concentrations of doxorubicin to the media. The 2D results indicated that doxorubicin effectively reduced the MCF-7 cell population at concentrations of approximately 0.1 μM (IC50 = 0.134 μM, Fig. 7A). On the contrary, all prototypes (G3A0.5, G3A1, G3A0.5C0.4, and G3A1C0.4) and Col1, exhibited significantly higher resistance to doxorubicin compared to the 2D model (IC50 > 100 μM), with no differences between Col1 and the prototypes. These differences in drug resistance between 2D and 3D models were already noted in other studies [13,112]. The capacity of 3D models to imitate the characteristics of the ECM facilitates the activation of drug resistance mechanisms in MCF-7. These results indicate that all the designed core-shell hydrogel beads exhibit significant potential as 3D BC models for testing chemotherapy agents and drug screening.

We also evaluated the expression of multidrug resistance (MDR) proteins in the designed prototypes, comparing them with the 2D model, to determine whether any differences were present (Fig. 7B), as well as the activation of these genes after incubation with doxorubicin (0.1 μM). First, we studied the expression of multidrug resistance-associated protein 1 (MRP1), encoded by ABCC1, and breast cancer resistance protein (BCRP), encoded by ABCG2. There was an under-expression of ABCC1 in G3A1C0.4, G3A0.5C0.4, and Col1, with no statistically significant difference between conditions. Moreover, this gene was not expressed in G3A1 and G3A0.5. On the contrary, ABCG2 was overexpressed in G3A1C0.4 and G3A0.5C0.4, underexpressed in G3A0.5 and Col1, and not expressed in G3A1. These results indicate that the presence of Col1 in the designed prototypes increases the expression of ABC efflux transporters. Collagen-mediated drug resistance has been previously observed, with studies showing that collagen activates the MAPK pathway, leading to the overexpression of ABC transporters [113,114].

We also examined the expression of Heat Shock Protein 90 Alpha Family Class A and B (HSP90AA1 and HSP90AB1), which are key regulators of cell autophagy and drug efflux, processes that enhance drug resistance [115,116]. The analysis of HSP90AA1 and HSP90AB1 expression showed a downregulation across all designed prototypes, suggesting that these drug resistance proteins are unlikely to be responsible for the doxorubicin resistance observed in this study. We also assessed the expression of CYP1A1, a cytochrome P450 enzyme involved in drug metabolism that is highly expressed in most BCs [117]. The prototypes that contain Col1 in the core overexpressed this marker, with G3A1C0.4 being the prototype with the highest expression. In addition, as doxorubicin acts by inhibiting topoisomerase II-α (TOP2A), and MCF-7 cells can evade this effect by downregulating the expression of this protein [118], we analyzed the expression of TOP2A in the designed prototypes. Despite there not being a statistical difference between conditions, the incorporation of Col1 revealed a tendency towards downregulation of this gene, a behavior associated with drug resistance. However, there were no differences between conditions, suggesting that the downregulation of this marker must be more linked

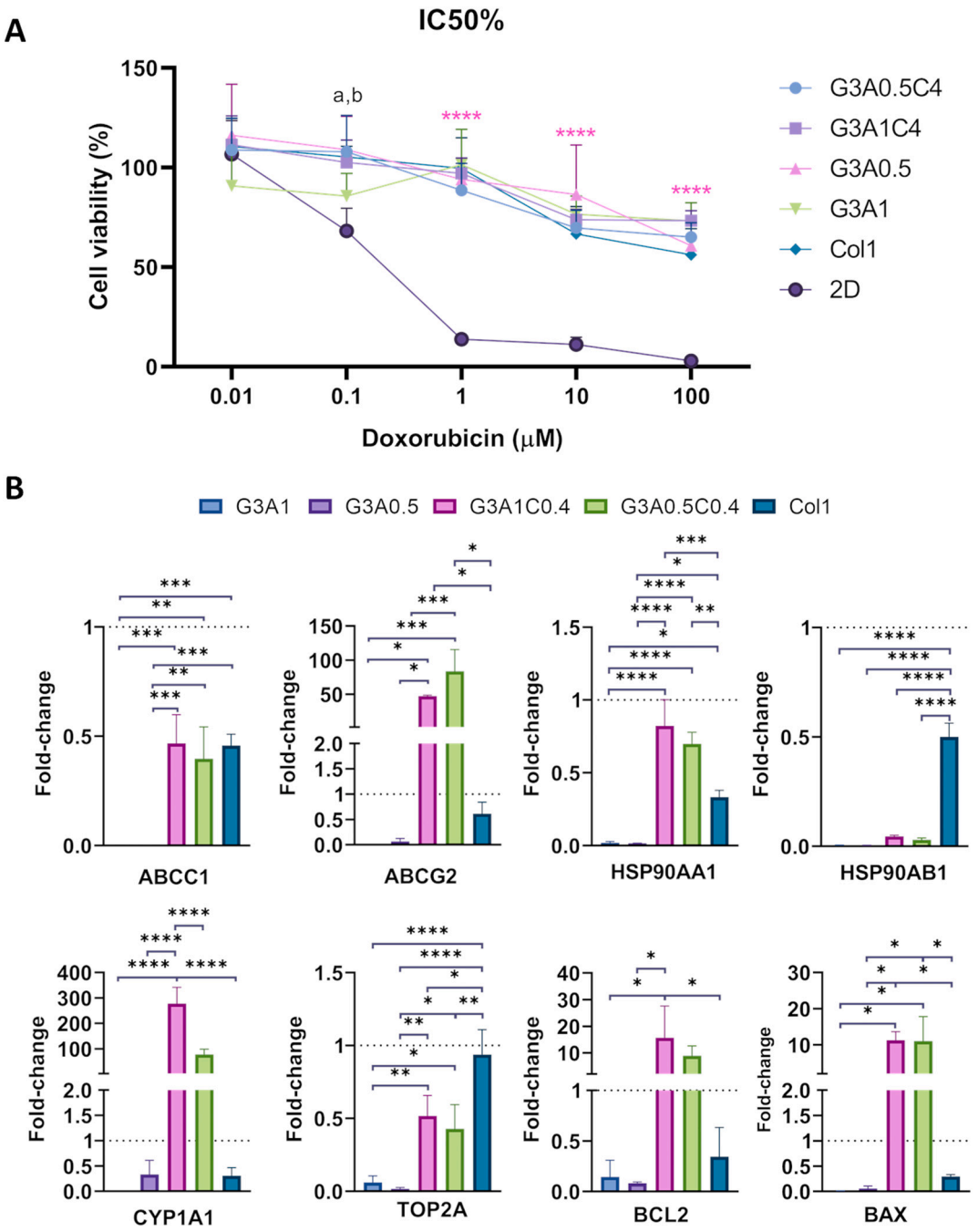

Fig. 7. Drug resistance analysis. (A) MCF-7 viability (%) after incubating core-shell hydrogel prototypes with different concentrations of doxorubicin for 48 h (Two-way ANOVA, $n_{G3A1} = 5$, $n_{G3A0.5,G3A1C0.4,G3A0.5C0.4,Col1,2D} = 6$; a: G3A1C0.4, Col1 *vs* 2D: $p < 0.01$; b: G3A0.5C0.4, G3A0.5 *vs* 2D: $p < 0.001$; pink asterisks: core-shell models and Col1 *vs* 2D). (B) Drug resistance marker genes (ABCC1, ABCG2, HSP90AA1, HSP90AB1, BAX, BCl2, TOP2A, CYP1A1) expression in MCF-7 grown in hydrogels G3A1, G3A1C0.4, G3A0.5, G3A0.5C0.4, and Col1 for 7 days. $2 - \Delta\Delta Ct$ values were calculated with the ΔCts from 2D cultures (One-way ANOVA, $N = 3$; *: $p < 0.05$, **: $p < 0.01$, ***: $p < 0.001$, ****: $p < 0.0001$). (For interpretation of the references to colour in this figure legend, the reader is referred to the web version of this article.)

to the 3D environment rather than the hydrogels' composition or mechanical properties.

Finally, as drug resistance is also mediated by the apoptosis pathway, the expression of the BCl-2 and BAX was assessed. BAX promotes apoptosis, and BCl-2 inhibits it [119]. During tumor progression, the expression of BCl-2 tends to increase, favoring cancer survival. BCl-2 binds to BAX, preventing its oligomerization, therefore, causing the death of BCCs [120]. In the prototypes designed, we observed that the addition of Col1 to the core was able to increase the expression of BCl-2 and BAX. Although these prototypes more accurately mimic the behavior of tumors *in vivo,* the anti-apoptotic effect was countered, meaning that apoptosis regulation was not the cause of the drug resistance observed in our prototypes.

These results indicate that the drug resistance observed in G3A1C0.4 and G3A0.5C0.4 is linked to the upregulation of ABCG2 and CYP1A1. However, in the case of G3A1 and G3A0.5 prototypes, it must be linked to the expression of different drug resistance markers, or to an increase in expression with exposure to drugs. We analyzed the expression of these markers after doxorubicin exposure, comparing the results with those obtained before treatment (Fig. S2). We observed an increase in

the expression of all drug resistance markers studied in the Col1 prototype, except for BAX. Moreover, an increase in the expression of both BAX and BCl-2 was observed in G3A1, G3A1C0.4, and G3A0.5C0.4. Despite this increase, the balance between these markers remained stable, indicating no significant variation in the apoptotic response. Nevertheless, the incorporation of Col1 into the core-shell hydrogels promoted the expression of drug resistance observed in BC, therefore suggesting that G3A1C0.4 and G3A0.5C0.4 could be suitable models for assessing the efficacy of anticancer therapeutics.

4. Conclusions

In this study, we engineered an advanced 3D *in vitro* BC model consisting of a core-shell hydrogel bead, which closely replicates the tumor's high Col1 content and stiffness. Additionally, the alginate shell creates a confined environment for BCC growth, reflecting the spatial restrictions encountered in DCIS tumors and thereby enhancing the physiological relevance of the model. Within these models, MCF-7 cells formed spheroids and cell aggregates with high proliferation and metabolic activity. The Col1 enrichment in the hydrogel beads' core enhanced the physiological relevance of these models by enabling them to express markers linked to malignancy, invasion, and drug resistance in BC *in vivo*. Remarkably, these 3D prototypes demonstrated significantly higher resistance to doxorubicin than conventional 2D cultures. Overall, Col1-enriched core-shell hydrogel beads have potential as translatable BC models due to their capability to emulate aggressive tumor phenotypes. Moreover, the preparation of core-shell hydrogel beads can be easily adapted to high-throughput fabrication and screening, providing a powerful tool in preclinical testing. Additionally, stromal cells such as macrophages or fibroblasts can be incorporated into the shell, allowing for the study of their interactions with BCCs, as well as endothelial cells, to evaluate angiogenesis within the model. The models could also serve as a platform for spheroid production, as the shell supports confined 3D growth and can be disrupted with calcium chelators to recover the spheroids for downstream experiments. The results suggest that G3A1C0.4 and G3A0.5C0.4 hold potential for BC modeling; however, certain limitations must be taken into account. Since the experiments were conducted using only one cell type (MCF-7), the findings may not be generalizable to other BC subtypes. Future studies using other BCCs and stromal cells are needed to validate the model's potential in reproducing the invasiveness and drug resistance occurring *in vivo*. Additionally, the diffusion of doxorubicin within the core-shell hydrogel beads was not evaluated, nor were other chemotherapy agents evaluated, to decipher the impact of limited drug diffusion or the drug mechanism of action might have on drug resistance within our model. The expression of markers associated with BCC malignancy and invasion was examined at the gene level; proteomic analyses may allow the identification and quantification of the proteins that are overexpressed in this model. Future research will help to demonstrate the capacity of these models to imitate human tumors, providing opportunities for therapeutic innovation.

CRediT authorship contribution statement

Uxia Gato-Diaz: Writing – original draft, Methodology, Investigation, Formal analysis, Data curation. **Lisandra de Castro-Alves:** Writing – review & editing, Methodology, Investigation. **Angel Concheiro:** Writing – review & editing, Validation, Funding acquisition, Conceptualization. **Yolanda Piñeiro:** Writing – review & editing, Methodology, Funding acquisition, Conceptualization. **Carmen Alvarez-Lorenzo:** Writing – review & editing, Validation, Supervision, Funding acquisition, Conceptualization. **Barbara Blanco-Fernandez:** Writing – review & editing, Visualization, Validation, Supervision, Methodology, Funding acquisition, Formal analysis, Data curation, Conceptualization. **José Rivas:** Writing – review & editing, Funding acquisition, Conceptualization.

Funding

This work was supported by the Strategic State Plan for Scientific, Technical, and Innovation Research MICIU/AEI/10.13039/501100011033, European Union NextGenerationEU/PRTR (PLEC2022–009217) by the Ministry of Science, Innovation, and Universities of Spain (to L.A., Y. P., and J.R.) and by ISCII through CERTERA, the State Network Consortium for the Development of Advanced Therapy Medicines (PERTE for Cutting-Edge Health, Recovery, Transformation and Resilience Plan, Proyect CERT22/00015). The work was also funded by the Xunta de Galicia (ED431F 2024/19 to B.B.F.; ED431C 2024/09: to B.B.F., C.A.L., A.C.); Ministry of Science, Innovation, and Universities of Spain MICIU/AEI/ 10.13039/50110001103 (PID2023-150422OB-I00 to A.C. and C.A.L.; PID2023-147892OA-I00 to B.B.F.), ERDF A way of making Europe, and the European Union; and MICIU/AEI/10.13039/501100011033 MICIU/AEI and FSE+ (RYC2022–037421-I to B.B.F.).

Declaration of competing interest

The authors declare that they have no known competing financial interests or personal relationships that could have appeared to influence the work reported in this paper.

Acknowledgements

Special thanks to Mercedes Rivas for her assistance in confocal microscopy at RIAIDT.

Appendix A. Supplementary data

Supplementary data to this article can be found online at https://doi.org/10.1016/j.ijbiomac.2025.149205.

Data availability

The data that support the findings of this study are available upon reasonable request from the corresponding authors.

References

[1] F. Bray, M. Laversanne, H. Sung, J. Ferlay, R.L. Siegel, I. Soerjomataram, A. Jemal, Global cancer statistics 2022: GLOBOCAN estimates of incidence and mortality worldwide for 36 cancers in 185 countries, CA Cancer J. Clin. 74 (2024) 229–263, https://doi.org/10.3322/caac.21834.
[2] World Health Organization, Breast cancer Fact Sheets. https://www.who.int/news-room/fact-sheets/detail/breast-cancer, 2024.
[3] J. Wang, B. Li, M. Luo, J. Huang, K. Zhang, S. Zheng, S. Zhang, J. Zhou, Progression from ductal carcinoma in situ to invasive breast cancer: molecular features and clinical significance, Signal Transduct. Target. Ther. 9 (2024) 83, https://doi.org/10.1038/s41392-024-01779-3.
[4] C. Toniatti, P. Jones, H. Graham, B. Pagliara, G. Draetta, Oncology drug discovery: planning a turnaround, Cancer Discov. 4 (2014) 397–404, https://doi.org/10.1158/2159-8290.CD-13-0452.
[5] G. Bağcı, C. Ximenes-Carballo, S. Perez-Amodio, O. Castaño, E. Engel, B. Blanco-Fernandez, Advanced 3D In Vitro Models to Recapitulate the Breast Tumor Microenvironment, 2022, pp. 193–232.
[6] S. Hong, J.M. Song, 3D bioprinted drug-resistant breast cancer spheroids for quantitative in situ evaluation of drug resistance, Acta Biomater. 138 (2022) 228–239, https://doi.org/10.1016/j.actbio.2021.10.031.
[7] K.P. Guillen, M. Fujita, A.J. Butterfield, S.D. Scherer, M.H. Bailey, Z. Chu, Y. S. DeRose, L. Zhao, E. Cortes-Sanchez, C.-H. Yang, et al., A human breast cancer-derived xenograft and organoid platform for drug discovery and precision oncology, Nat. Can. 3 (2022) 232–250, https://doi.org/10.1038/s43018-022-00337-6.
[8] L. Broutier, G. Mastrogiovanni, M.M. Verstegen, H.E. Francies, L.M. Gavarró, C. R. Bradshaw, G.E. Allen, R. Arnes-Benito, O. Sidorova, M.P. Gaspersz, et al., Human primary liver cancer–derived organoid cultures for disease modeling and drug screening, Nat. Med. 23 (2017) 1424–1435, https://doi.org/10.1038/nm.4438.
[9] S. Vanni, T.M. Caputo, A.M. Cusano, A. De Vita, A. Cusano, C. Cocchi, C. Mulè, S. Principe, C. Liverani, G. Celetti, et al., Engineered anti-HER2 drug delivery

nanosystems for the treatment of breast cancer, Nanoscale 17 (2025) 9436–9457, https://doi.org/10.1039/D4NR03907F.
[10] A. Rodallec, G. Sicard, S. Giacometti, M. Carré, B. Pourroy, F. Bouquet, A. Savina, B. Lacarelle, J. Ciccolini, R. Fanciullino, From 3D spheroids to tumor bearing mice: efficacy and distribution studies of trastuzumab-docetaxel immunoliposome in breast cancer, Int. J. Nanomedicine 13 (2018) 6677–6688, https://doi.org/10.2147/IJN.S179290.
[11] B. Blanco-Fernandez, V.M. Gaspar, E. Engel, J.F. Mano, Proteinaceous hydrogels for bioengineering advanced 3D tumor models. Advanced, Science (2021) 8, https://doi.org/10.1002/advs.202003129.
[12] J. Insua-Rodríguez, T. Oskarsson, The extracellular matrix in breast cancer, Adv. Drug Deliv. Rev. 97 (2016) 41–55, https://doi.org/10.1016/j.addr.2015.12.017.
[13] E. Henke, R. Nandigama, S. Ergün, Extracellular matrix in the tumor microenvironment and its impact on Cancer therapy, Front. Mol. Biosci. (2020) 6, https://doi.org/10.3389/fmolb.2019.00160.
[14] S. Mittal, N.J. Brown, I. Holen, The breast tumor microenvironment: role in cancer development, progression and response to therapy, Expert. Rev. Mol. Diagn. 18 (2018) 227–243, https://doi.org/10.1080/14737159.2018.1439382.
[15] A. Quarta, N. Gallo, D. Vergara, L. Salvatore, C. Nobile, A. Ragusa, A. Gaballo, Investigation on the composition of agarose–collagen i blended hydrogels as matrices for the growth of spheroids from breast cancer cell lines, Pharmaceutics 13 (2021) 963, https://doi.org/10.3390/pharmaceutics13070963.
[16] H. Saini, K. Rahmani Eliato, C. Silva, M. Allam, G. Mouneimne, R. Ros, M. Nikkhah, The role of Desmoplasia and stromal fibroblasts on anti-cancer drug resistance in a microengineered tumor model, Cell. Mol. Bioeng. 11 (2018) 419–433, https://doi.org/10.1007/s12195-018-0544-9.
[17] L. Cassereau, Y.A. Miroshnikova, G. Ou, J. Lakins, V.M. Weaver, A 3D tension bioreactor platform to study the interplay between ECM stiffness and tumor phenotype, J. Biotechnol. 193 (2015) 66–69, https://doi.org/10.1016/j.jbiotec.2014.11.008.
[18] W. Sun, C.T. Lim, N.A. Kurniawan, Mechanistic adaptability of cancer cells strongly affects anti-migratory drug efficacy, J. R. Soc. Interface 11 (2014) 20140638, https://doi.org/10.1098/rsif.2014.0638.
[19] J. Redmond, H.O. McCarthy, P. Buchanan, T.J. Levingstone, N.J. Dunne, Development and characterisation of 3D collagen-gelatin based scaffolds for breast cancer research, Biomaterials Advances. 142 (2022) 213157, https://doi.org/10.1016/j.bioadv.2022.213157.
[20] A.D. Arya, P.M. Hallur, A.G. Karkisaval, A. Gudipati, S. Rajendiran, V. Dhavale, B. Ramachandran, A. Jayaprakash, N. Gundiah, A. Chaubey, Gelatin methacrylate hydrogels as biomimetic three-dimensional matrixes for modeling breast Cancer invasion and Chemoresponse in vitro, ACS Appl. Mater. Interfaces 8 (2016) 22005–22017, https://doi.org/10.1021/acsami.6b06309.
[21] S. De, N. Singh, Collagen-alginate 3D microscaffolds for studying cellular migration, Int. J. Biol. Macromol. 245 (2023) 125308, https://doi.org/10.1016/j.ijbiomac.2023.125308.
[22] C. Liu, D. Lewin Mejia, B. Chiang, K.E. Luker, G.D. Luker, Hybrid collagen alginate hydrogel as a platform for 3D tumor spheroid invasion, Acta Biomater. 75 (2018) 213–225, https://doi.org/10.1016/j.actbio.2018.06.003.
[23] T. Jiang, J.G. Munguia-Lopez, K. Gu, M.M. Bavoux, S. Flores-Torres, J. Kort-Mascort, J. Grant, S. Vijayakumar, A. De Leon-Rodriguez, A.J. Ehrlicher, et al., Engineering bioprintable alginate/gelatin composite hydrogels with tunable mechanical and cell adhesive properties to modulate tumor spheroid growth kinetics, Biofabrication 12 (2019) 015024, https://doi.org/10.1088/1758-5090/ab3a5c.
[24] Y. Man, Tumor cell budding from focally disrupted tumor capsules: a common pathway for all breast cancer subtype derived invasion? J. Cancer (2010) 32–37, https://doi.org/10.7150/jca.1.32.
[25] N. Rajan, J. Habermehl, M.-F. Coté, C.J. Doillon, D. Mantovani, Preparation of ready-to-use, storable and reconstituted type I collagen from rat tail tendon for tissue engineering applications, Nat. Protoc. 1 (2006) 2753–2758, https://doi.org/10.1038/nprot.2006.430.
[26] B. Blanco-Fernandez, S. Rey-Vinolas, G. Bagci, G. Rubi-Sans, J. Otero, D. Navajas, S. Perez-Amodio, E. Engel, Bioprinting decellularized breast tissue for the development of 3D breast cancer models, ACS Appl. Mater. Interfaces 14 (2022) 29467–29482, https://doi.org/10.1021/acsami.2c00920.
[27] J. Schindelin, I. Arganda-Carreras, E. Frise, V. Kaynig, M. Longair, T. Pietzsch, S. Preibisch, C. Rueden, S. Saalfeld, B. Schmid, et al., Fiji: an open-source platform for biological-image analysis, Nat. Methods 9 (2012) 676–682, https://doi.org/10.1038/nmeth.2019.
[28] L.-L. Liu, H. Zhao, T.-F. Ma, F. Ge, C.-S. Chen, Y.-P. Zhang, Identification of valid reference genes for the normalization of RT-qPCR expression studies in human breast Cancer cell lines treated with and without transient transfection, PLoS One 10 (2015) e0117058, https://doi.org/10.1371/journal.pone.0117058.
[29] X. Dai, L. Liu, J. Ouyang, X. Li, X. Zhang, Q. Lan, T. Xu, Coaxial 3D bioprinting of self-assembled multicellular heterogeneous tumor fibers, Sci. Rep. 7 (2017) 1457, https://doi.org/10.1038/s41598-017-01581-y.
[30] K. Alessandri, B.R. Sarangi, V.V. Gurchenkov, B. Sinha, T.R. Kießling, L. Fetler, F. Rico, S. Scheuring, C. Lamaze, A. Simon, et al., Cellular capsules as a tool for multicellular spheroid production and for investigating the mechanics of tumor progression in vitro, Proc. Natl. Acad. Sci. 110 (2013) 14843–14848, https://doi.org/10.1073/pnas.1309482110.
[31] J.H. Yeon, S.H. Chung, C. Baek, H. Hwang, J. Min, A simple pipetting-based method for encapsulating live cells into multi-layered hydrogel droplets, Biochip J. 12 (2018) 184–192, https://doi.org/10.1007/s13206-018-2307-z.
[32] L. Yu, S.M. Grist, S.S. Nasseri, E. Cheng, Y.-C.E. Hwang, C. Ni, K.C. Cheung, Core-shell hydrogel beads with extracellular matrix for tumor spheroid formation, Biomicrofluidics (2015) 9, https://doi.org/10.1063/1.4918754.
[33] P. Agarwal, H. Wang, M. Sun, J. Xu, S. Zhao, Z. Liu, K.J. Gooch, Y. Zhao, X. Lu, X. He, Microfluidics enabled bottom-up engineering of 3D vascularized tumor for drug discovery, ACS Nano 11 (2017) 6691–6702, https://doi.org/10.1021/acsnano.7b00824.
[34] J.M. Northcott, I.S. Dean, J.K. Mouw, V.M. Weaver, Feeling stress: the mechanics of Cancer progression and aggression. Front cell, Dev. Biol. (2018) 6, https://doi.org/10.3389/fcell.2018.00017.
[35] A.L. Correia, M.J. Bissell, The tumor microenvironment is a dominant force in multidrug resistance, Drug Resist. Updat. 15 (2012) 39–49, https://doi.org/10.1016/j.drup.2012.01.006.
[36] M.J. Paszek, N. Zahir, K.R. Johnson, J.N. Lakins, G.I. Rozenberg, A. Gefen, C. A. Reinhart-King, S.S. Margulies, M. Dembo, D. Boettiger, et al., Tensional homeostasis and the malignant phenotype, Cancer Cell 8 (2005) 241–254, https://doi.org/10.1016/j.ccr.2005.08.010.
[37] E.O. Osidak, P.A. Karalkin, M.S. Osidak, V.A. Parfenov, D.E. Sivogrivov, F.D.A. S. Pereira, A.A. Gryadunova, E.V. Koudan, Y.D. Khesuani, V.A. Kasyanov, et al., Viscoll collagen solution as a novel bioink for direct 3D bioprinting, J. Mater. Sci. Mater. Med. 30 (2019) 31, https://doi.org/10.1007/s10856-019-6233-y.
[38] A. Svanström, J. Rosendahl, S. Salerno, M.C. Leiva, P. Gregersson, M. Berglin, Y. Bogestål, J. Lausmaa, A. Oko, G. Chinga-Carrasco, et al., Optimized alginate-based 3D printed scaffolds as a model of patient derived breast cancer microenvironments in drug discovery, Biomed. Mater. 16 (2021) 045046, https://doi.org/10.1088/1748-605X/ac0451.
[39] P. Ren, D. Wei, M. Liang, L. Xu, T. Zhang, Q. Zhang, Alginate/gelatin-based hybrid hydrogels with function of injecting and encapsulating cells in situ, Int. J. Biol. Macromol. 212 (2022) 67–84, https://doi.org/10.1016/j.ijbiomac.2022.05.058.
[40] C.S. Szot, C.F. Buchanan, J.W. Freeman, M.N. Rylander, 3D in vitro bioengineered tumors based on collagen I hydrogels, Biomaterials 32 (2011) 7905–7912, https://doi.org/10.1016/j.biomaterials.2011.07.001.
[41] S. Xu, H. Xu, W. Wang, S. Li, H. Li, T. Li, W. Zhang, X. Yu, L. Liu, The role of collagen in cancer: from bench to bedside, J. Transl. Med. 17 (2019) 309, https://doi.org/10.1186/s12967-019-2058-1.
[42] R. Yerushalmi, R. Woods, P.M. Ravdin, M.M. Hayes, K.A. Gelmon, Ki67 in breast cancer: prognostic and predictive potential, Lancet Oncol. 11 (2010) 174–183, https://doi.org/10.1016/S1470-2045(09)70262-1.
[43] M. Cavo, M. Fato, L. Peñuela, F. Beltrame, R. Raiteri, S. Scaglione, Microenvironment complexity and matrix stiffness regulate breast cancer cell activity in a 3D in vitro model, Sci. Rep. 6 (2016) 35367, https://doi.org/10.1038/srep35367.
[44] Y. Liang, J. Jeong, R.J. DeVolder, C. Cha, F. Wang, Y.W. Tong, H. Kong, A cell-instructive hydrogel to regulate malignancy of 3D tumor spheroids with matrix rigidity, Biomaterials 32 (2011) 9308–9315, https://doi.org/10.1016/j.biomaterials.2011.08.045.
[45] C. Hoffmann, X. Mao, J. Brown-Clay, F. Moreau, A. Al Absi, H. Wurzer, B. Sousa, F. Schmitt, G. Berchem, B. Janji, et al., Hypoxia promotes breast cancer cell invasion through HIF-1α-mediated up-regulation of the invadopodial actin bundling protein CSRP2, Sci. Rep. 8 (2018) 10191, https://doi.org/10.1038/s41598-018-28637-x.
[46] S. Linder, P. Cervero, R. Eddy, J. Condeelis, Mechanisms and roles of podosomes and invadopodia, Nat. Rev. Mol. Cell Biol. 24 (2023) 86–106, https://doi.org/10.1038/s41580-022-00530-6.
[47] L.M. Machesky, Lamellipodia and filopodia in metastasis and invasion, FEBS Lett. 582 (2008) 2102–2111, https://doi.org/10.1016/j.febslet.2008.03.039.
[48] L. Chen, Z. Xiao, Y. Meng, Y. Zhao, J. Han, G. Su, B. Chen, J. Dai, The enhancement of cancer stem cell properties of MCF-7 cells in 3D collagen scaffolds for modeling of cancer and anti-cancer drugs, Biomaterials 33 (2012) 1437–1444, https://doi.org/10.1016/j.biomaterials.2011.10.056.
[49] O. Ilina, P.G. Gritsenko, S. Syga, J. Lippoldt, C.A.M. La Porta, O. Chepizhko, S. Grosser, M. Vullings, G.-J. Bakker, J. Starruß, et al., Cell–cell adhesion and 3D matrix confinement determine jamming transitions in breast cancer invasion, Nat. Cell Biol. 22 (2020) 1103–1115, https://doi.org/10.1038/s41556-020-0552-6.
[50] A.L. Harris, Hypoxia — a key regulatory factor in tumour growth, Nat. Rev. Cancer 2 (2002) 38–47, https://doi.org/10.1038/nrc704.
[51] C. Hoffmann, X. Mao, M. Dieterle, F. Moreau, A. Al Absi, A. Steinmetz, A. Oudin, G. Berchem, B. Janji, C. Thomas, CRP2, a new invadopodia actin bundling factor critically promotes breast cancer cell invasion and metastasis, Oncotarget 7 (2016) 13688–13705, https://doi.org/10.18632/oncotarget.7327.
[52] R. Suresh, R.J. Diaz, The remodelling of actin composition as a hallmark of cancer, Transl. Oncol. 14 (2021) 101051, https://doi.org/10.1016/j.tranon.2021.101051.
[53] I. Ayala, M. Baldassarre, G. Caldieri, R. Buccione, Invadopodia: A guided tour, Eur. J. Cell Biol. 85 (2006) 159–164, https://doi.org/10.1016/j.ejcb.2005.09.005.
[54] E.S. Clark, A.S. Whigham, W.G. Yarbrough, A.M. Weaver, Cortactin is an essential regulator of matrix metalloproteinase secretion and extracellular matrix degradation in Invadopodia, Cancer Res. 67 (2007) 4227–4235, https://doi.org/10.1158/0008-5472.CAN-06-3928.
[55] M.A. Khajah, Y.A. Luqmani, Involvement of membrane Blebbing in immunological disorders and Cancer, Med. Princ. Pract. 25 (2016) 18–27, https://doi.org/10.1159/000441848.

[56] G.T. Charras, C.-K. Hu, M. Coughlin, T.J. Mitchison, Reassembly of contractile actin cortex in cell blebs, J. Cell Biol. 175 (2006) 477–490, https://doi.org/10.1083/jcb.200602085.
[57] J.S. Nielsen, M.L. Graves, S. Chelliah, A.W. Vogl, C.D. Roskelley, K.M. McNagny, The CD34-related molecule Podocalyxin is a potent inducer of microvillus formation, PLoS One 2 (2007) e237, https://doi.org/10.1371/journal.pone.0000237.
[58] K.A. Snyder, M.R. Hughes, B. Hedberg, J. Brandon, D.C. Hernaez, P. Bergqvist, F. Cruz, K. Po, M.L. Graves, M.E. Turvey, et al., Podocalyxin enhances breast tumor growth and metastasis and is a target for monoclonal antibody therapy, Breast Cancer Res. 17 (2015) 46, https://doi.org/10.1186/s13058-015-0562-7.
[59] D.A. Applewhite, M. Barzik, S. Kojima, T.M. Svitkina, F.B. Gertler, G.G. Borisy, Ena/VASP proteins have an anti-capping independent function in Filopodia formation, Mol. Biol. Cell 18 (2007) 2579–2591, https://doi.org/10.1091/mbc.e06-11-0990.
[60] A.J. Berger, C.M. Renner, I. Hale, X. Yang, S.M. Ponik, P.S. Weisman, K. S. Masters, P.K. Kreeger, Scaffold stiffness influences breast cancer cell invasion via EGFR-linked Mena upregulation and matrix remodeling, Matrix Biol. 85–86 (2020) 80–93, https://doi.org/10.1016/j.matbio.2019.07.006.
[61] X. Li, X. Sun, C. Kan, B. Chen, N. Qu, N. Hou, Y. Liu, F. Han, COL1A1: A novel oncogenic gene and therapeutic target in malignancies, Pathol. Res. Pract. 236 (2022) 154013, https://doi.org/10.1016/j.prp.2022.154013.
[62] G. Corso, J. Figueiredo, S. De Angelis, Corso F. Pietro, A. Girardi, J. Pereira, R. Seruca, B. Bonanni, P. Carneiro, G. Pravettoni, et al., E-cadherin deregulation in breast cancer, J. Cell. Mol. Med. 24 (2020) 5930–5936, https://doi.org/10.1111/jcmm.15140.
[63] G. Breier, M. Grosser, M. Rezaei, Endothelial cadherins in cancer, Cell Tissue Res. 355 (2014) 523–527, https://doi.org/10.1007/s00441-014-1851-7.
[64] D.E. White, W.J. Muller, Multifaceted roles of Integrins in breast Cancer metastasis, J. Mammary Gland Biol. Neoplasia 12 (2007) 135–142, https://doi.org/10.1007/s10911-007-9045-5.
[65] W. Guo, F.G. Giancotti, Integrin signalling during tumour progression, Nat. Rev. Mol. Cell Biol. 5 (2004) 816–826, https://doi.org/10.1038/nrm1490.
[66] M.N.O. Moritz, A.R. Merkel, E.G. Feldman, H.S. Selistre-de-Araujo, Rhoades (Sterling) JA., Biphasic α2β1 integrin expression in breast Cancer metastasis to bone, Int. J. Mol. Sci. 22 (2021) 6906, https://doi.org/10.3390/ijms22136906.
[67] J.-M. Nam, Y. Onodera, M.J. Bissell, C.C. Park, Breast Cancer cells in three-dimensional culture display an enhanced Radioresponse after coordinate targeting of integrin α5β1 and fibronectin, Cancer Res. 70 (2010) 5238–5248, https://doi.org/10.1158/0008-5472.CAN-09-2319.
[68] H. Hamidi, J. Ivaska, Every step of the way: integrins in cancer progression and metastasis, Nat. Rev. Cancer 18 (2018) 533–548, https://doi.org/10.1038/s41568-018-0038-z.
[69] X. Li, L. Zhao, C. Chen, J. Nie, B. Jiao, Can EGFR be a therapeutic target in breast cancer? Biochimica et Biophysica Acta (BBA) - reviews on, Cancer 1877 (2022) 188789, https://doi.org/10.1016/j.bbcan.2022.188789.
[70] C.R. Chong, P.A. Jänne, The quest to overcome resistance to EGFR-targeted therapies in cancer, Nat. Med. 19 (2013) 1389–1400, https://doi.org/10.1038/nm.3388.
[71] R. Wise, A. Zolkiewska, Metalloprotease-dependent activation of EGFR modulates CD44+/CD24− populations in triple negative breast cancer cells through the MEK/ERK pathway, Breast Cancer Res. Treat. 166 (2017) 421–433, https://doi.org/10.1007/s10549-017-4440-0.
[72] T.C. Rao, V.P.-Y. Ma, A. Blanchard, T.M. Urner, S. Grandhi, K. Salaita, A. L. Mattheyses, EGFR activation attenuates the mechanical threshold for integrin tension and focal adhesion formation, J. Cell Sci. (2020) 133, https://doi.org/10.1242/jcs.238840.
[73] C.C. Mader, M. Oser, M.A.O. Magalhaes, J.J. Bravo-Cordero, J. Condeelis, A. J. Koleske, H. Gil-Henn, An EGFR–Src–Arg–Cortactin pathway mediates functional maturation of Invadopodia and breast Cancer cell invasion, Cancer Res. 71 (2011) 1730–1741, https://doi.org/10.1158/0008-5472.CAN-10-1432.
[74] Y. Zhang, J. Li, X.-N. Lai, X.-Q. Jiao, J.-P. Xiong, L.-X. Xiong, Focus on Cdc42 in breast Cancer: new insights, target therapy development and non-coding RNAs, Cells 8 (2019) 146, https://doi.org/10.3390/cells8020146.
[75] K. Stengel, Y. Zheng, Cdc42 in oncogenic transformation, invasion, and tumorigenesis, Cell. Signal. 23 (2011) 1415–1423, https://doi.org/10.1016/j.cellsig.2011.04.001.
[76] S. Lakshmi, T.A. Hughes, S. Priya, Exosomes and exosomal RNAs in breast cancer: A status update, Eur. J. Cancer 144 (2021) 252–268, https://doi.org/10.1016/j.ejca.2020.11.033.
[77] J. Winkler, A. Abisoye-Ogunniyan, K.J. Metcalf, Z. Werb, Concepts of extracellular matrix remodelling in tumour progression and metastasis, Nat. Commun. 11 (2020) 5120, https://doi.org/10.1038/s41467-020-18794-x.
[78] S. Kaushik, M.W. Pickup, V.M. Weaver, From transformation to metastasis: deconstructing the extracellular matrix in breast cancer, Cancer Metastasis Rev. 35 (2016) 655–667, https://doi.org/10.1007/s10555-016-9650-0.
[79] A. Parnigoni, P. Moretto, M. Viola, E. Karousou, A. Passi, D. Vigetti, Effects of Hyaluronan on breast Cancer aggressiveness, Cancers (Basel) 15 (2023) 3813, https://doi.org/10.3390/cancers15153813.
[80] J.Y. Lee, O. Chaudhuri, Regulation of breast Cancer progression by extracellular matrix mechanics: insights from 3D culture models, ACS Biomater Sci. Eng. 4 (2018) 302–313, https://doi.org/10.1021/acsbiomaterials.7b00071.
[81] D.T. Butcher, T. Alliston, V.M. Weaver, A tense situation: forcing tumour progression, Nat. Rev. Cancer 9 (2009) 108–122, https://doi.org/10.1038/nrc2544.
[82] M. Kodaka, Y. Hata, The mammalian hippo pathway: regulation and function of YAP1 and TAZ, Cell. Mol. Life Sci. 72 (2015) 285–306, https://doi.org/10.1007/s00018-014-1742-9.
[83] L. Wu, X. Yang, Targeting the hippo pathway for breast Cancer therapy, Cancers (Basel) 10 (2018) 422, https://doi.org/10.3390/cancers10110422.
[84] J. Fu, W. Liu, S. Liu, R. Zhao, T. Hayashi, H. Zhao, Y. Xiang, K. Mizuno, S. Hattori, H. Fujisaki, et al., Inhibition of YAP/TAZ pathway contributes to the cytotoxicity of silibinin in MCF-7 and MDA-MB-231 human breast cancer cells, Cell. Signal. 119 (2024) 111186, https://doi.org/10.1016/j.cellsig.2024.111186.
[85] P.D. Talukdar, H. Roy, U. Chatterji, Targeting breast cancer stem cells in ER-positive breast cancer by repurposing the benzoporphyrin derivative verteporfin as a YAP/TAZ small molecule inhibitor, Mol. Biol. Rep. 52 (2025) 154, https://doi.org/10.1007/s11033-025-10264-1.
[86] M. Maugeri-Saccà, M. Barba, L. Pizzuti, P. Vici, L. Di Lauro, R. Dattilo, I. Vitale, M. Bartucci, M. Mottolese, R. De Maria, The hippo transducers TAZ and YAP in breast cancer: oncogenic activities and clinical implications, Expert Rev. Mol. Med. 17 (2015) e14, https://doi.org/10.1017/erm.2015.12.
[87] M. Shibata, K. Ham, M.O. Hoque, A time for YAP1: tumorigenesis, immunosuppression and targeted therapy, Int. J. Cancer 143 (2018) 2133–2144, https://doi.org/10.1002/ijc.31561.
[88] S.W. Chan, C.J. Lim, K. Guo, C.P. Ng, I. Lee, W. Hunziker, Q. Zeng, W. Hong, A role for TAZ in migration, invasion, and tumorigenesis of breast Cancer cells, Cancer Res. 68 (2008) 2592–2598, https://doi.org/10.1158/0008-5472.CAN-07-2696.
[89] S. Dupont, L. Morsut, M. Aragona, E. Enzo, S. Giulitti, M. Cordenonsi, F. Zanconato, J. Le Digabel, M. Forcato, S. Bicciato, et al., Role of YAP/TAZ in mechanotransduction, Nature 474 (2011) 179–183, https://doi.org/10.1038/nature10137.
[90] G. Brusatin, T. Panciera, A. Gandin, A. Citron, S. Piccolo, Biomaterials and engineered microenvironments to control YAP/TAZ-dependent cell behaviour, Nat. Mater. 17 (2018) 1063–1075, https://doi.org/10.1038/s41563-018-0180-8.
[91] T. Panciera, L. Azzolin, M. Cordenonsi, S. Piccolo, Mechanobiology of YAP and TAZ in physiology and disease, Nat. Rev. Mol. Cell Biol. 18 (2017) 758–770, https://doi.org/10.1038/nrm.2017.87.
[92] J. Luo, H. Zou, Y. Guo, T. Tong, Y. Chen, Y. Xiao, Y. Pan, P. Li, The oncogenic roles and clinical implications of YAP/TAZ in breast cancer, Br. J. Cancer 128 (2023) 1611–1624, https://doi.org/10.1038/s41416-023-02182-5.
[93] B.G. Hollier, A.A. Tinnirello, S.J. Werden, K.W. Evans, J.H. Taube, T.R. Sarkar, N. Sphyris, M. Shariati, S.V. Kumar, V.L. Battula, et al., FOXC2 expression links epithelial–mesenchymal transition and stem cell properties in breast cancer, Cancer Res. 73 (2013) 1981–1992, https://doi.org/10.1158/0008-5472.CAN-12-2962.
[94] M. Katoh, M. Igarashi, H. Fukuda, H. Nakagama, M. Katoh, Cancer genetics and genomics of human FOX family genes, Cancer Lett. 328 (2013) 198–206, https://doi.org/10.1016/j.canlet.2012.09.017.
[95] K.M. Hargadon, E.W. Strong, The FOXC2 transcription factor: A master regulator of Chemoresistance in Cancer, Technol. Cancer Res. Treat. (2023) 22, https://doi.org/10.1177/15330338231155284.
[96] H.D. Tran, K. Luitel, M. Kim, K. Zhang, G.D. Longmore, D.D. Tran, Transient SNAIL1 expression is necessary for metastatic competence in breast Cancer, Cancer Res. 74 (2014) 6330–6340, https://doi.org/10.1158/0008-5472.CAN-14-0923.
[97] K. Lundgren, B. Nordenskjöld, G. Landberg, Hypoxia, snail and incomplete epithelial–mesenchymal transition in breast cancer, Br. J. Cancer 101 (2009) 1769–1781, https://doi.org/10.1038/sj.bjc.6605369.
[98] A.G. de Herreros, S. Peiró, M. Nassour, P. Savagner, Snail family regulation and epithelial mesenchymal transitions in breast Cancer progression, J. Mammary Gland Biol. Neoplasia 15 (2010) 135–147, https://doi.org/10.1007/s10911-010-9179-8.
[99] J.E. Curran, S.R. Weinstein, L.R. Griffiths, Polymorphic variants of NFKB1 and its inhibitory protein NFKBIA, and their involvement in sporadic breast cancer, Cancer Lett. 188 (2002) 103–107, https://doi.org/10.1016/S0304-3835(02)00460-3.
[100] E. Pavitra, J. Kancharla, V.K. Gupta, K. Prasad, J.Y. Sung, J. Kim, M.B. Tej, R. Choi, J.-H. Lee, Y.-K. Han, et al., The role of NF-κB in breast cancer initiation, growth, metastasis, and resistance to chemotherapy, Biomed. Pharmacother. 163 (2023) 114822, https://doi.org/10.1016/j.biopha.2023.114822.
[101] K. Shostak, A. Chariot, NF-κB, stem cells and breast cancer: the links get stronger, Breast Cancer Res. 13 (2011) 214, https://doi.org/10.1186/bcr2886.
[102] M. Luo, J.-L. Guan, Focal adhesion kinase: A prominent determinant in breast cancer initiation, progression and metastasis, Cancer Lett. 289 (2010) 127–139, https://doi.org/10.1016/j.canlet.2009.07.005.
[103] S. Hehlgans, M. Haase, N. Cordes, Signalling via integrins: implications for cell survival and anticancer strategies. Biochimica et Biophysica Acta (BBA) - reviews on, Cancer (2007) 163–180, https://doi.org/10.1016/j.bbcan.2006.09.001, 1775.
[104] K.R. Levental, H. Yu, L. Kass, J.N. Lakins, M. Egeblad, J.T. Erler, S.F.T. Fong, K. Csiszar, A. Giaccia, W. Weninger, et al., Matrix crosslinking forces tumor progression by enhancing integrin signaling, Cell 139 (2009) 891–906, https://doi.org/10.1016/j.cell.2009.10.027.
[105] M.A. Eckert, J. Yang, Targeting invadopodia to block breast cancer metastasis, Oncotarget 2 (2011) 562–568, https://doi.org/10.18632/oncotarget.301.
[106] J.G. Habib, J.A. O'Shaughnessy, The hedgehog pathway in triple-negative breast cancer, Cancer Med. 5 (2016) 2989–3006, https://doi.org/10.1002/cam4.833.

[107] M.F. Barginear, M. Leung, D.R. Budman, The hedgehog pathway as a therapeutic target for treatment of breast cancer, Breast Cancer Res. Treat. 116 (2009) 239–246, https://doi.org/10.1007/s10549-009-0423-0.
[108] Y. Katoh, M. Katoh, Hedgehog target genes: mechanisms of carcinogenesis induced by aberrant hedgehog signaling activation, Curr. Mol. Med. 9 (2009) 873–886, https://doi.org/10.2174/156652409789105570.
[109] S.S. Sikandar, A.H. Kuo, T. Kalisky, S. Cai, M. Zabala, R.W. Hsieh, N.A. Lobo, F. A. Scheeren, S. Sim, D. Qian, et al., Role of epithelial to mesenchymal transition associated genes in mammary gland regeneration and breast tumorigenesis, Nat. Commun. 8 (2017) 1669, https://doi.org/10.1038/s41467-017-01666-2.
[110] N.A. D'Angelo, M.A. Noronha, M.C.C. Câmara, I.S. Kurnik, C. Feng, V.H.S. Araujo, J.H.P.M. Santos, V. Feitosa, J.V.D. Molino, C.O. Rangel-Yagui, et al., Doxorubicin nanoformulations on therapy against cancer: an overview from the last 10 years, Biomaterials Advances. 133 (2022) 112623, https://doi.org/10.1016/j.msec.2021.112623.
[111] A. Sommer, A. Hermawan, B. Ljepoja, Frohlich T, Arnold G, Wagner E, Roidl A., A proteomic analysis of chemoresistance development via sequential treatment with doxorubicin reveals novel players in MCF-7 breast cancer cells, Int. J. Mol. Med. (2018), https://doi.org/10.3892/ijmm.2018.3781.
[112] M.V. Monteiro, V.M. Gaspar, L.P. Ferreira, J.F. Mano, Hydrogel 3D *in vitro* tumor models for screening cell aggregation mediated drug response, Biomater. Sci. 8 (2020) 1855–1864, https://doi.org/10.1039/C9BM02075F.
[113] F. Baltes, J. Caspers, S. Henze, M. Schlesinger, G. Bendas, Targeting Discoidin domain receptor 1 (DDR1) signaling and its crosstalk with β1-integrin emerges as a key factor for breast Cancer Chemosensitization upon collagen type 1 binding, Int. J. Mol. Sci. 21 (2020) 4956, https://doi.org/10.3390/ijms21144956.
[114] F. Baltes, V. Pfeifer, K. Silbermann, J. Caspers, K. Wantoch von Rekowski, M. Schlesinger, G. Bendas, β1-integrin binding to collagen type 1 transmits breast cancer cells into chemoresistance by activating ABC efflux transporters. Biochimica et Biophysica Acta (BBA) - molecular, Cell Res. 1867 (2020) 118663, https://doi.org/10.1016/j.bbamcr.2020.118663.
[115] P. Kumar, B. Devaki, U.K. Jonnala, Subbarao S. Amere, Hsp90 facilitates acquired drug resistance of tumor cells through cholesterol modulation however independent of tumor progression. Biochimica et Biophysica Acta (BBA) - molecular, Cell Res. 1867 (2020) 118728, https://doi.org/10.1016/j.bbamcr.2020.118728.
[116] X. Xiao, W. Wang, Y. Li, D. Yang, X. Li, C. Shen, Y. Liu, X. Ke, S. Guo, Z. Guo, HSP90AA1-mediated autophagy promotes drug resistance in osteosarcoma, J. Exp. Clin. Cancer Res. 37 (2018) 201, https://doi.org/10.1186/s13046-018-0880-6.
[117] M. Rodriguez, D.A. Potter, CYP1A1 regulates breast Cancer proliferation and survival, Mol. Cancer Res. 11 (2013) 780–792, https://doi.org/10.1158/1541-7786.MCR-12-0675.
[118] S. AbuHammad, M. Zihlif, Gene expression alterations in doxorubicin resistant MCF7 breast cancer cell line, Genomics 101 (2013) 213–220, https://doi.org/10.1016/j.ygeno.2012.11.009.
[119] S. Cory, J.M. Adams, The Bcl2 family: regulators of the cellular life-or-death switch, Nat. Rev. Cancer 2 (2002) 647–656, https://doi.org/10.1038/nrc883.
[120] D. Merino, S.W. Lok, J.E. Visvader, G.J. Lindeman, Targeting BCL-2 to enhance vulnerability to therapy in estrogen receptor-positive breast cancer, Oncogene 35 (2016) 1877–1887, https://doi.org/10.1038/onc.2015.287.